Cis-cis and *trans-perp* HOONO: Action spectroscopy and isomerization kinetics

Juliane L. Fry[a)]
Arthur Amos Noyes Laboratory of Chemical Physics, California Institute of Technology, Pasadena, California 91125

Sergey A. Nizkorodov
Department of Chemistry, University of California at Irvine, Irvine, California 92697

Mitchio Okumura[b)]
Arthur Amos Noyes Laboratory of Chemical Physics, California Institute of Technology, Pasadena, California 91125

Coleen M. Roehl
Division of Geological and Planetary Sciences, California Institute of Technology, Pasadena, California 91125

Joseph S. Francisco
Department of Chemistry, Purdue University, West Lafayette, Indiana 47907

Paul O. Wennberg[c)]
Division of Geological and Planetary Sciences and Division of Engineering and Applied Science, California Institute of Technology, Pasadena, California 91125

(Received 26 January 2004; accepted 21 April 2004)

The weakly bound HOONO product of the $OH+NO_2+M$ reaction is studied using the vibrational predissociation that follows excitation of the first OH overtone ($2\nu_1$). We observe formation of both *cis-cis* and *trans-perp* conformers of HOONO. The *trans-perp* HOONO $2\nu_1$ band is observed under thermal (223–238 K) conditions at 6971 cm^{-1}. We assign the previously published (warmer temperature) HOONO spectrum to the $2\nu_1$ band at 6365 cm^{-1} and $2\nu_1$-containing combination bands of the *cis-cis* conformer of HOONO. The band shape of the *trans-perp* HOONO spectrum is in excellent agreement with the predicted rotational contour based on previous experimental and theoretical results, but the apparent origin of the *cis-cis* HOONO spectrum at 6365 cm^{-1} is featureless and significantly broader, suggesting more rapid intramolecular vibrational redistribution or predissociation in the latter isomer. The thermally less stable *trans-perp* HOONO isomerizes rapidly to *cis-cis* HOONO with an experimentally determined lifetime of 39 ms at 233 K at 13 hPa (in a buffer gas of predominantly Ar). The temperature dependence of the *trans-perp* HOONO lifetime in the range 223–238 K yields an isomerization barrier of 33 ± 12 kJ/mol. New *ab initio* calculations of the structure and vibrational mode frequencies of the transition state *perp-perp* HOONO are performed using the coupled cluster singles and doubles with perturbative triples [CCSD(T)] model, using a correlation consistent polarized triple ζ basis set (cc-pVTZ). The energetics of *cis-cis*, *trans-perp*, and *perp-perp* HOONO are also calculated at this level [CCSD(T)/cc-pVTZ] and with a quadruple ζ basis set using the structure determined at the triple ζ basis set [CCSD(T)/cc-pVQZ//CCSD(T)/cc-pVTZ]. These calculations predict that the *anti* form of *perp-perp* HOONO has an energy of $\Delta E_0=42.4$ kJ/mol above *trans-perp* HOONO, corresponding to an activation enthalpy of $\Delta H_{298}^{\ddagger 0}=41.1$ kJ/mol. These results are in good agreement with statistical simulations based on a model developed by Golden, Barker, and Lohr. The simulated isomerization rates match the observed decay rates when modeled with a *trans-perp* to *cis-cis* HOONO isomerization barrier of 40.8 kJ/mol and a strong collision model. The quantum yield of *cis-cis* HOONO dissociation to OH and NO_2 is also calculated as a function of photon excitation energy in the range 3500–7500 cm^{-1}, assuming $D_0=83$ kJ/mol. The quantum yield is predicted to vary from 0.15 to 1 over the observed spectrum at 298 K, leading to band intensities in the action spectrum that are highly temperature dependent; however, the observed relative band strengths in the *cis-cis* HOONO spectrum do not change substantially with temperature over the range 193–273 K. Semiempirical calculations of the oscillator strengths for $2\nu_1$(*cis-cis* HOONO) and $2\nu_1$(*trans-perp* HOONO) are performed using (1) a one-dimensional anharmonic model and (2)

[a)]Author to whom correspondence should be addressed; Electronic mail. fry@caltech.edu
[b)]Author to whom correspondence should be addressed; Electronic mail. mo@caltech.edu
[c)]Author to whom correspondence should be addressed; Electronic mail. wennberg@gps.caltech.edu

a Morse oscillator model for the OH stretch, and *ab initio* dipole moment functions calculated using Becke, Lee, Yang, and Parr density functional theory (B3LYP), Møller-Plesset pertubation theory truncated at the second and third order (MP2 and MP3), and quadratic configuration interaction theory using single and double excitations (QCISD). The QCISD level calculated ratio of $2\nu_1$ oscillator strengths of *trans-perp* to *cis-cis* HOONO is 3.7:1. The observed intensities indicate that the concentration of *trans-perp* HOONO early in the $OH+NO_2$ reaction is significantly greater than predicted by a Boltzmann distribution, consistent with statistical predictions of high initial yields of *trans-perp* HOONO from the $OH+NO_2+M$ reaction. In the atmosphere, *trans-perp* HOONO will isomerize nearly instantaneously to *cis-cis* HOONO. Loss of HOONO via photodissociation in the near-IR limits the lifetime of *cis-cis* HOONO during daylight to less than 45 h, other loss mechanisms will reduce the lifetime further. © *2004 American Institute of Physics.*
[DOI: 10.1063/1.1760714]

I. INTRODUCTION

Knowledge of the concentrations and chemistry of the HO_x ($OH+HO_2$) and NO_x ($NO+NO_2$) families of radicals is central to understanding global atmospheric chemistry. Both families are involved in tropospheric ozone production and stratospheric ozone loss. Hydroxyl radical (OH) has extremely high reactivity with many atmospheric trace gases, and is referred to as an atmospheric detergent because it cleanses the atmosphere of pollutants. NO_x is a major component of photochemical smog.

As the major sink of both HO_x and NO_x, the radical termination reaction

$$OH+NO_2+M\rightarrow HONO_2+M \tag{1}$$

is of critical importance in atmospheric chemistry. The rate constant of this reaction has been the topic of some controversy[1–7] because the high and low pressure rate constants could not be reconciled with a single termolecular rate expression. This discrepancy can be resolved by the inclusion of a second minor channel forming a more weakly bound isomer of nitric acid, peroxynitrous acid, or HOONO, as first predicted by Robertshaw and Smith:[8]

$$OH+NO_2+M\rightarrow HONO_2+M \tag{1a}$$

$$\rightarrow HOONO+M. \tag{1b}$$

The energetics of $OH+NO\rightarrow HOONO$ and $HONO_2$ are shown in Fig. 1, with relative *cis-cis*, *trans-perp*, and *perp-perp* HOONO energies from CCSD(T)/cc-pVQZ/CCSD(T)/cc-pVTZ [where CCSD(T)—coupled cluster singles and doubles with perturbative triples, cc-pVTZ—correlation consistent polarized triple ζ basis set, and cc-pVQZ—correlation consistent quadruple ζ basis set] level calculations reported in this paper. The energies of $OH+NO_2$ and $HONO_2$ relative to *cis-cis* HOONO are taken from Bean *et al.*[9] The formation of HOONO instead of $HONO_2$ has very different implications for the atmospheric concentrations of OH and NO_2. Since HOONO is more weakly bound than $HONO_2$ (Fig. 1), it will have a short lifetime (on the order of seconds at 300 K) in the lower atmosphere due to efficient thermal dissociation back to OH and NO_2. No evidence has yet been found for direct isomerization of HOONO into $HONO_2$,[7] and it is likely to be prevented by a high reaction barrier.[10] A majority of previous kinetics studies of reaction (1) were done via observation of OH decay in the presence of excess NO_2 without taking the HOONO channel into consideration. At some conditions, these experiments measured the total reaction rate coefficient, $k_1=k_{1a}+k_{1b}$, while assuming the observed decay was due only to k_{1a}. Recent measurements[3,9,11] have found that HOONO is indeed formed in reaction (1) with a measurable yield of $k_{1b}/(k_{1a}+k_{1b})\approx 5-10\%$ at low pressures (27 hPa) and room temperature. Thus, to the extent that HOONO is formed, the total rate of reaction (1) overestimates the net loss of HO_x and NO_x to HNO_3.

The $OH+NO_2$ system is complicated by the existence of several distinct conformers of HOONO.[1,12–14] The predicted lowest-energy conformers are *cis-cis* and *trans-perp* HOONO (Fig. 1), wherein the first and second prefixes refer to the conformations of the ONOO and NOOH dihedral angles, respectively. The planar *cis-cis* conformer has a weak internal hydrogen bond and is computed to be stabilized relative to the open *trans-perp* conformer by 15.3 kJ/mol. A third conformer, *cis-perp* HOONO, was identified in early *ab initio* calculations of McGrath and Rowland[12] and calculated to be 1.7–2.5 kJ/mol above *cis-cis* HOONO. Tsai *et al.*[14] and Jin *et al.*[13] have calculated *cis-perp* HOONO energies (relative to *cis-cis* HOONO) of 3.8–5.4 kJ/mol and −5.1–5.9 kJ/mol, respectively. Recent higher-level calculations indicate that the *cis-perp* conformer may not be a stationary point on the HOONO potential energy surface.[2,10]

Isomerization between the *trans-perp* and *cis-cis* conformers of HOONO occurs by rotation about the N-O bond.

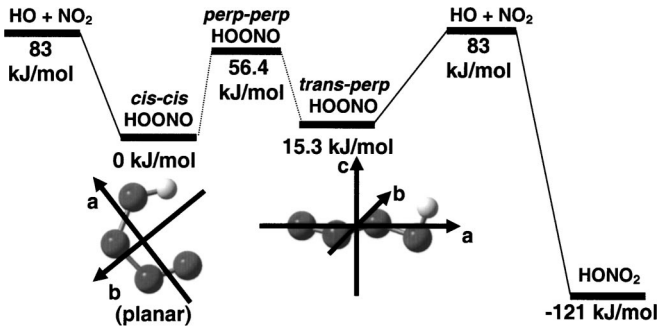

FIG. 1. Energy level diagram for the $OH+NO_2$ reaction, with structures of *trans-perp* and *cis-cis* HOONO shown. HOONO energy levels are from present work; $HONO_2$ energy relative to *cis-cis* HOONO are from Bean *et al.*[9] and $OH+NO_2$ energy relative to *cis-cis* HOONO is from Hippler, Nasterlack, and Striebel[3] and Dixon *et al.*[10] Pathways for direct isomerization from HOONO into $HONO_2$ are not shown because they have substantially higher barriers compared to dissociation into OH and NO_2.

This transition state was first termed *perp-perp* HOONO by McGrath and Rowland,[12] because the OH and NO bonds are nearly perpendicular to the O-O-N plane. They calculated a transition state energy of 52.3 kJ/mol above the *cis-cis* conformer of HOONO. There are predicted to be two *perp-perp* conformers, encompassing two transition states of nearly identical energies and similar structures and frequencies. In the *anti* configuration, the OH and NO bonds lie on opposite sides of the NOO plane, in the *syn* conformation, they are on the same side. Golden, Barker, and Lohr,[2] Jin *et al.*,[13] and Tsai *et al.*[14] have found that the two *perp-perp* HOONO conformers have nearly identical energetics. This has led Golden, Barker, and Lohr[2] to treat the isomerization from *trans-perp* to *cis-cis* HOONO as occurring by a single pathway with a degeneracy of two in statistical calculations.

Vibrational frequencies of various conformers of HOONO have been predicted at several levels of theory. MP2/6-31G(d) calculations (where MP2—Møller-Plesset theory truncated at the second order) of the harmonic vibrational frequencies and infrared intensities of eight conformational structures of HOONO were carried out by McGrath and Rowland.[12] Li and Francisco[15] later calculated vibrational frequencies for *cis-cis* HOONO at the QCISD(T)/cc-pVTZ level (where QCISD—quadratic configuration interaction theory using single and double excitations), and Jin *et al.*[13] reported vibrational frequencies for nine structures of HOONO (including the two *perp-perp* conformers) at the B3LYP/6-311+G(d,p) and MP2/6-311+G(d,p) levels (where B3LYP—Becke, Lee, Yang, and Parr density functional theory). Bean *et al.*[9] reported vibrational frequencies for both *cis-cis* and *trans-perp* HOONO at the CCSD(T)/cc-pVTZ level.

Estimates of the dissociation energy of *cis-cis* HOONO are converging on a value between 76 and 84 kJ/mol. Among the most recent *ab initio* calculations of the dissociation energy, Li and Francisco calculate D_0(*cis-cis* HOONO) $=78.7$ kJ/mol at the QCISD(T)/cc-pVQZ level, and Dixon *et al.* calculate two values for D_0(*cis-cis* HOONO): first, 82.9 kJ/mol, a strictly *ab initio* number calculated at the CCSD(T)/CBS (where CBS—complete basis set) level with core/valence corrections to the dissociation energy and molecular scalar relativistic corrections accounting for the change in relativistic contributions to the total energy of the molecular or radical species versus the constituent atoms; second, 76.6 kJ/mol, using an experimental value for $\Delta H_f(\mathrm{NO_2})$. These calculations give a 6 kJ/mol wide bracket for the value of D_0(*cis-cis* HOONO), the width of which demonstrates the uncertainty of the *ab initio* calculations. Hippler, Nasterlack, and Striebel report the only experimental value, D_0(*cis-cis* HOONO) $=83$ kJ/mol, from a third-law analysis of the equilibrium constants over 430–490 K.[3] A refinement of the evaluation of this data is underway, and reanalysis of the high temperature data now gives $D_0(cis\text{-}cis\ \mathrm{HOONO}) = 80.5$ kJ/mol.[16] Pollack *et al.*[17] have set an experimental upper limit on the *trans-perp* HOONO binding energy of 70.3 kJ/mol from the product internal energy distribution of the vibrational predissociation of jet-cooled *trans-perp* HOONO. From this limit and the *ab initio* energy difference between *cis-cis* and *trans-perp* HOONO, they find an upper limit for the *cis-cis* HOONO dissociation energy, D_0(*cis-cis* HOONO) $\leqslant 84.6$ kJ/mol.

There have been several statistical calculations modeling the pressure and temperature dependence and HOONO/$\mathrm{HONO_2}$ branching ratio of this reaction.[4,5,18] In the most recent study, Golden, Barker, and Lohr[2] have published a thorough multiwell, multichannel master equation model of the $\mathrm{OH}+\mathrm{NO_2}$ system. Their modeling is consistent with previous experimental results, but all such calculations still rely on experimental constraints and cannot predict the behavior of this reaction from first principles.

The first spectroscopic observation of HOONO was a matrix study by Cheng, Lee, and Lee[19] identifying several fundamental bands (700–3600 $\mathrm{cm^{-1}}$) of both *cis-cis* and *trans-perp* HOONO after photolysis of $\mathrm{HONO_2}$ in an Ar matrix. The first observation of HOONO in the gas phase was the action spectroscopy experiment reported by Nizkorodov and Wennberg[11] in 2002. In this method, HOONO is excited in the first overtone region by near-IR photons to predissociating states; absorption is monitored by laser-induced fluorescence (LIF) detection of OH products formed upon dissociation to OH and $\mathrm{NO_2}$. They observed a series of vibrational bands in the first OH overtone spectral range from products of reaction (1) occurring in a flowing discharge cell, and provided tentative assignments of the bands in terms of the three conformers of HOONO.

The work of Nizkorodov and Wennberg was followed by observation of the OH stretching fundamental of *cis-cis* HOONO at 3306 $\mathrm{cm^{-1}}$ in direct absorption by cavity ring down spectroscopy.[9] Bean *et al.* determined the yield of HOONO in reaction (1) by directly measuring the integrated vibrational bands of *cis-cis* HOONO and $\mathrm{HONO_2}$; however, they were unable to detect *trans-perp* isomer because its spectrum is obscured by the strong nitric acid band. They assumed, with support from statistical calculations, that any *trans-perp* HOONO formed in reaction (1) had isomerized to *cis-cis* HOONO in their experiment. Subsequently, Pollack *et al.* definitively identified the first OH stretching overtone of supersonically cooled *trans-perp* HOONO from the rotational band contours detected with photodissociation action spectroscopy.[17] Though the band origin at 6971.4 $\mathrm{cm^{-1}}$ lies close to the strongest band seen by Nizkorodov and Wennberg, the band is expected to be substantially narrower even at room temperature.

Several key issues remain unresolved, chief among them the question of whether *trans-perp* HOONO is produced in reaction (1) under thermal conditions. Statistical calculations indicate that this isomer will be formed in a high, nonthermal yield from this reaction; if so, then what is its spectroscopic signature, and how rapidly does it isomerize to *cis-cis* HOONO? The assignment of the bands seen in the HOONO overtone action spectrum reported by Nizkorodov and Wennberg remains unclear, especially given the new spectroscopic studies and recent *ab initio* studies suggesting that *cis-perp* HOONO structure is not stable.[2,10] If the spectrum is assigned to the *cis-cis* HOONO conformer, then the dissociation energy D_0 of this conformer is critical for interpreting the action spectrum, since the action spectrum requires that

the molecule undergo vibrational predissociation to OH $+NO_2$ after absorption of a near-IR photon. Current estimates of the dissociation energy are greater than the photon energy for most of the observed bands, implying that the quantum yield is less than unity for much of the spectrum.

In this paper, we reexamine the spectroscopy and isomerization kinetics of HOONO conformers in a discharge flow cell using the predissociation action spectroscopy approach of Nizkorodov and Wennberg. The goal of this study is to reconcile all of the spectroscopic measurements and to provide experimental and theoretical results on the relative energies and reaction barriers on the HOONO potential energy surface. Specifically, we seek to detect the conformers of HOONO by action spectroscopy, and to measure directly the rate and activation energy for isomerization of *trans-perp* HOONO to *cis-cis* HOONO. We apply statistical RRKM (Rice-Ramsperger-Kassel-Marcus) theory to calculate the isomerization rates, for comparison to the experimental data, and to predict photodissociation quantum yield of *cis-cis* HOONO to $OH+NO_2$. We perform CCSD(T) calculations to improve on predictions of the structure, energy, and frequencies of the isomerization transition state (*anti* configuration of the *perp-perp* HOONO structure), and refine the relative energetics of the *cis-cis*, *trans-perp*, and (*anti*-)*perp-perp* HOONO conformers. Finally, we calculate the oscillator strengths of both stable conformers, *cis-cis* and *trans-perp* HOONO. The calculated intensities allow us to estimate the *cis-cis* and *trans-perp* HOONO yields in our experiment, and to predict the lifetime of HOONO in the atmosphere due to predissociation by near-IR radiation.

II. EXPERIMENTAL DETAILS

A. Action spectroscopy

We investigate the spectroscopy and isomerization kinetics of HOONO conformers using photodissociation action spectroscopy. In this method, HOONO undergoes vibrational predissociation upon absorption of a near-IR photon. The excitation is to the first overtone of the OH stretch vibration ($2\nu_1$), and the resulting OH fragment is detected via LIF. This technique combines molecular selectivity with very high sensitivity: The more stable isomer of nitric acid, $HONO_2$, will not dissociate at this energy, and the LIF method is sensitive to as few as 10^4 OH molecules/cm^3.[20] The experimental apparatus consists of two synchronized lasers to produce the pump (IR) and probe (UV) pulses, a flow cell and reaction chamber, and a photon-counting photomultiplier tube (PMT) detector mounted above the gas flow and lasers. A schematic overview is shown in Fig. 2.

B. Flow cell and generation of OH radicals and HOONO

Gases are mixed in a 50 cm temperature controlled jacketed glass flow cell of 25 mm internal diameter. The flow cell has a movable injector, and the interior is coated with Teflon to minimize the occurrence of heterogeneous chemistry on the walls.

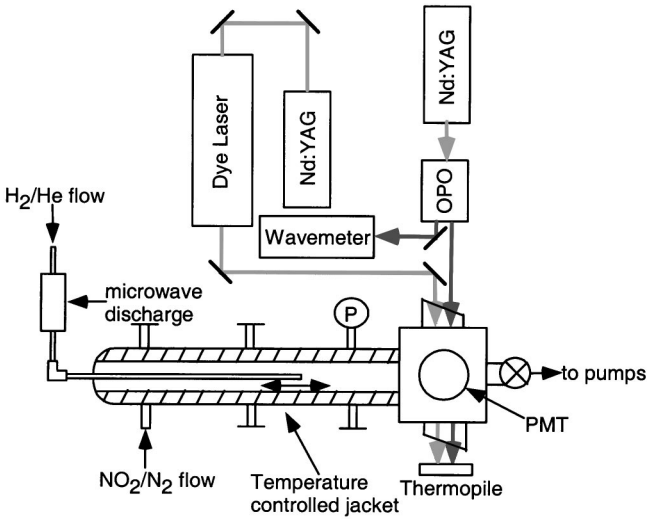

FIG. 2. Schematic of the experimental apparatus. The pulsed (100 Hz) tunable infrared (1.3–1.6 μm) for photolysis of HOONO and pulsed tunable ultraviolet (280–285 nm) for OH LIF enter the detection chamber perpendicular to the gas flow. A PMT detector, behind a 311 nm bandpass filter, at 90° to the flows and the lasers, detects the OH LIF. HOONO is produced in a temperature controlled (200–280 K) flow cell via gas-phase chemistry. The time delay between the formation of HOONO and its detection can be varied by adjusting the flow rate and position of the H-atom injector.

In a 2450 MHz McCarroll cavity microwave discharge, H_2 gas is converted to H atoms in the presence of buffer Ar. The H atoms react to form OH radicals rapidly upon mixing with flow containing NO_2:

$$H+NO_2 \rightarrow OH+NO \tag{2}$$

The OH quickly reacts with another NO_2 molecule, forming nitric acid and HOONO conformers [reactions (1a) and (1b)]. Under optimized conditions, the flow cell pressure is 13 hPa and the flow consists of 300 SCCM (SCCM denotes cubic centimeter per minute at STP) Ar and 60 SCCM 1% H_2 in He through the discharge mixed with 50 SCCM 4% NO_2 in N_2. This corresponds to 1.5% H_2, 0.5% NO_2, 72% Ar, 14% He, and 12% N_2.

The reaction $OH+NO_2+M \rightarrow HNO_3+M$ occurs on a microsecond time scale in the temperature range 200–280 K of the flow cell. At the injector port, however, the local temperature of the mixing gases is higher than the controlled flow cell wall temperature due to the highly exothermic reactions (2) and (1). We cannot, therefore, quantitatively treat the formation kinetics of HOONO. This is not a concern in the experiments reported here, since the isomerization kinetics take place on a longer time scale (60–90 ms).

C. Lasers and detection

Reaction products are probed in a laser interaction region downstream from the injector at a distance which varies from 20 to 40 cm. The flowing gas is crossed by two lasers, an infrared laser for vibrational overtone excitation followed by a UV laser to probe OH products by laser induced fluorescence.

The tunable near IR is generated in a type-II beta-BaB_2O_4 (BBO) optical parametric oscillator (OPO) pumped by the 355 nm third harmonic of a pulsed Nd:YAG (yttrium aluminum garnet) laser (3 cm^{-1} bandwidth). This

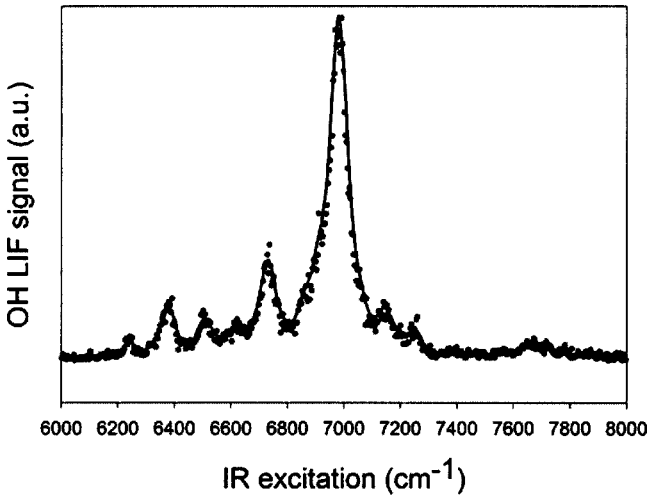

FIG. 3. Averaged HOONO action spectrum obtained at $T=213$ K, $P=13$ hPa. Previously unobserved features at 6250, 6971, and 7700 cm^{-1} are seen in the spectrum.

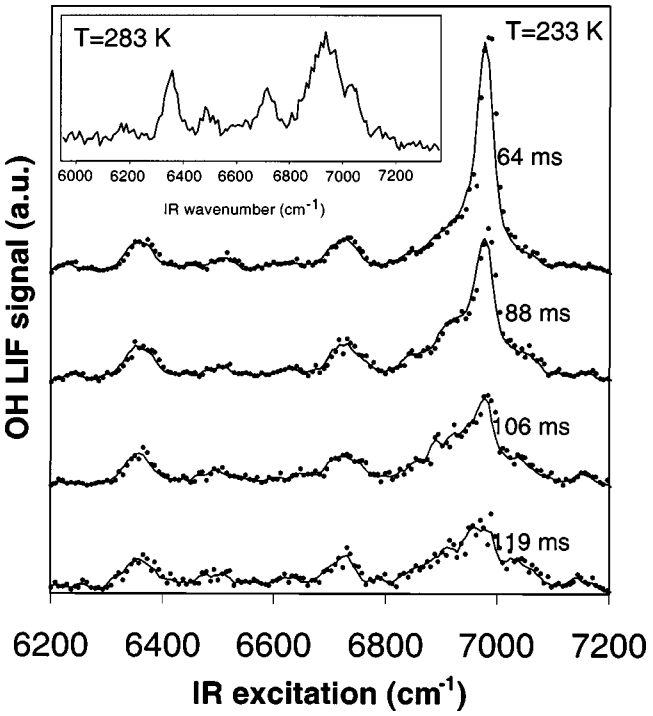

FIG. 4. HOONO action spectra at various flow cell residence times obtained at $T=233$ K, $P=13$ hPa. Three spectra have been averaged at each residence time, and all spectra are scaled to the same 6365 cm^{-1} peak intensity. The prominent band at 6971 cm^{-1} is assigned to *trans-perp* HOONO. The *trans-perp* HOONO band decays relative to the *cis-cis* HOONO band on the ~100 ms time scale. Inset: 283 K spectrum of the same region contains *cis-cis* HOONO bands only. This spectrum was obtained with flow conditions and averaging identical to the $T=233$ K spectra.

OPO (Ref. 21) outputs 2–3 mJ/pulse in the idler beam, tunable in the range 800–2500 nm (4000–12 500 cm^{-1}) by rotation of the BBO crystals. The frequency of the signal beam is continuously monitored by a pulsed wavemeter. The wavemeter calibration is verified using photoacoustic spectroscopy of the well-known water transitions in the 7000–7200 cm^{-1} region.[22]

The IR pump beam passes through the detection chamber via Brewster-angle CaF_2 windows, perpendicular to the gas flow, and is measured by a thermal power meter after exiting the chamber for calibration of laser power fluctuations. It is overlapped spatially with the UV output of a second laser system, the second harmonic of a Rhodamine 6G dye laser pumped by a frequency doubled Nd:YAG laser (~0.2 cm^{-1} bandwidth).

The UV beam (<1 μJ, tunable 280–282 nm) excites OH in the $A\,^2\Sigma(v=1)\leftarrow X\,^2\Pi(v=0)$ band. The $A\,^2\Sigma(v=1)$ OH relaxes via collisions to the $v=0$ state and fluorescence is observed at 309 nm $[A\,^2\Sigma(v=0)\rightarrow X\,^2\Pi(v=0)]$. The LIF signal is focused onto a bialkali photomultiplier tube mounted above the detection region, at right angles to both the laser beams and the gas flow. A narrow band filter with 6 nm transmission bandwidth centered at 310 nm is employed to reject scattered UV and visible laser light.

For the data reported here, several modes of data acquisition are used. In the pump scanning mode, the IR pump beam is scanned over the $2\nu_1$ region of the HOONO spectrum, while the UV probe beam is maintained tuned on the strongest OH LIF feature $[Q_{21}(1)+Q_{11}(1)+R_{22}(3)$ unresolved triplet of lines]. This yields action spectra, such as Figs. 3–5, in which the signal at each wavelength is proportional to the product of the absorption cross section and the quantum yield for photodissociation. In this mode, the pump-probe delay is set to 1 μs. This ensures a thermalized OH distribution, so that relative quantum yields from different bands are unaffected by differences in initially formed OH rotational state distribution. In the probe scanning mode, used to measure OH product state distribution shown in Fig. 6, the IR pump beam is tuned to a wavelength corresponding to a particular overtone band of the molecule of interest, and the UV LIF probe beam is scanned over several OH features corresponding to different N states of the photolysis product OH. In this mode, the pump-probe timing is set to the minimum possible delay, 50 ns, to capture the nascent OH rotational state distribution. Because of the 50 ns delay between pump and probe beams and the relatively high flow cell pressure, 13 hPa, the measured OH product state distribution is some what relaxed by rotational energy transfer from the nascent OH distribution produced in photodissociation. However, qualitative differentiation between chemical species is still possible. In the flow kinetics mode, used to generate Fig. 7, the IR pump beam is toggled between three wavelengths of interest corresponding to various combinations of the two conformers. The subsequent data analysis to obtain isomerization lifetimes is described below in Sec. III C. Again, the UV probe beam is tuned on the strongest OH LIF feature. Results of all three modes of operation described above will be reported below.

III. EXPERIMENTAL RESULTS

A. New transient *trans-perp* HOONO spectrum

At room temperature, we observe the same spectrum previously reported by Nizkorodov and Wennberg.[11] However, upon cooling the flow cell to below 243 K, a new spectral feature emerges on top of the earlier spectrum (Fig. 3). The feature is centered at 6971 cm^{-1} with a width of ~30 cm^{-1}, substantially narrower than the bands seen in the room

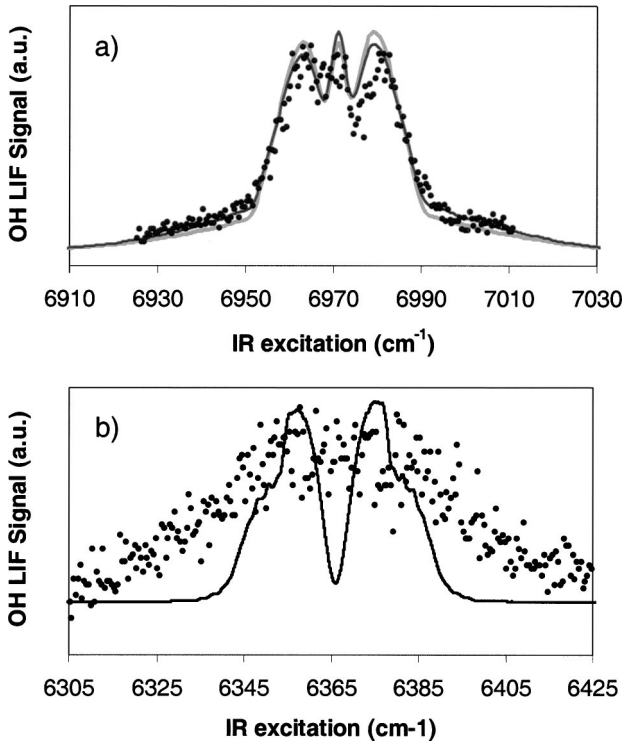

FIG. 5. (a) Action spectrum of *trans-perp* HOONO at 213 K. A slow scan (0.05 cm^{-1} step size; 3 cm^{-1} resolution) over the narrow peak in Fig. 3 reveals band structure. Smooth lines are simulations from the program ASYROTWIN (Ref. 23) using molecular parameters from Table I. Black and gray solid lines are band simulations for an *a*-type to *c*-type ratio of 1.8 and 1, respectively. The *a*-type/*c*-type ratio of 1.8 is the hybrid band type calculated in this paper; while the *a*-type/*c*-type ratio of 1 is the approximate band type for *trans-perp* HOONO found by Pollack *et al.* to best represent their experimental spectrum in a supersonic expansion. (b) Action spectrum of $2\nu_1$ band of *cis-cis* HOONO at 273 K. A slow scan (points) reveals no resolvable structure. Line is a simulation of a pure *b*-type transition, using the program ASYROTWIN (Ref. 23) with *cis-cis* HOONO molecular parameters from Table I.

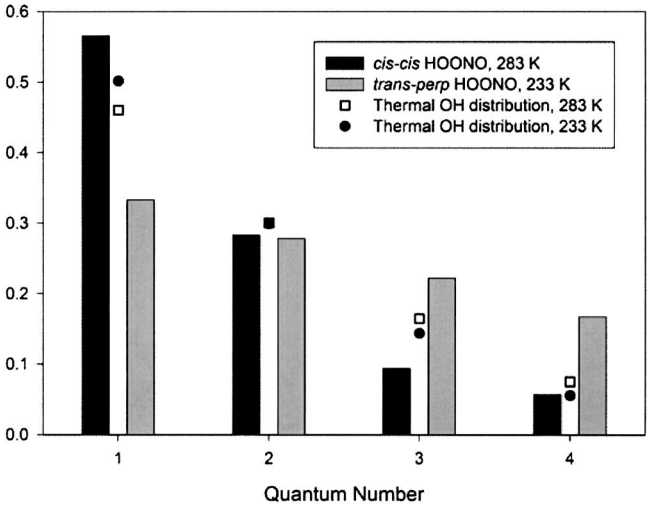

FIG. 6. Relative populations of the first few OH $^2\Pi_{3/2}^-(N)$ rotational states, $N=1-4$. Black bars represent normalized population of the lowest quantum states after IR photodissociation on a *cis-cis* HOONO band at 6365 cm^{-1} at 283 K; gray bars, after photodissociation on a *trans-perp* HOONO band at 6970 cm^{-1} at 233 K. Both *cis-cis* and *trans-perp* HOONO measurements were conducted at 13 hPa, 50 ns pump-probe delay. Symbols indicate thermal OH distribution at the two temperatures. Large difference in the OH fragment internal energy reflects the difference in the photon energy available for dissociation.

temperature spectrum. Figure 3 shows an averaged spectrum of HOONO at 213 K. With decreasing temperature, this band rapidly grows in intensity relative to the other observed bands. The relative intensity of this feature also depends on the time delay between mixing H and NO_2 inside the flow cell and detection of HOONO in the main chamber. The apparent lifetime of the narrow band at this temperature is in the 100 ms range (Fig. 4). The transient nature of this feature is consistent with a less stable conformer of HOONO, which isomerizes to a more stable conformer or undergoes some other reaction on a millisecond time scale. The peak position is consistent with the overtone frequency predicted for the free OH bond in *trans-perp* conformer of HOONO and the overtone band recently fit as *trans-perp* HOONO in a pulsed supersonic expansion (5 K) by Pollack *et al.*[17] We therefore assign this new spectrum to the *trans-perp* conformer of HOONO.

This assignment can be confirmed by examination of the observed band shape. Figure 5(a) shows a 3 cm^{-1} resolution action spectrum of the 6971 cm^{-1} peak at 213 K along with rotational band contour simulations performed with the ASYROTWIN program.[23] We used the calculated rotational constants shown in Table I and assumed the same constants for upper and lower states, in a mixed *a*-type and *c*-type hybrid band. The first simulation [dark line, Fig. 5(a)], which used the *a*-type to *c*-type ratio of 1.8 derived from *ab initio* calculations of the *trans-perp* HOONO overtone transition moments discussed in Sec. IV D, matches our 213 K flow cell spectrum very well. Also shown for comparison is a simulation with an *a*-type to *c*-type band ratio of 1, a ratio which Pollack *et al.*[17] found to give the best representation of their 5 K spectrum of *trans-perp* HOONO [gray line, Fig. 5(a)].

In the room temperature spectrum, all of the subbands behave similarly with respect to changes in chemistry and temperature. This multiple-band spectrum is present without

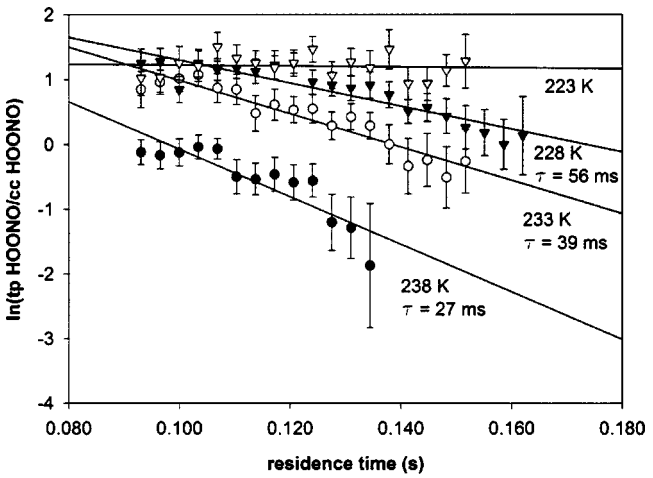

FIG. 7. Measurement of lifetimes of *trans-perp* HOONO in the flow cell at various temperatures. The measurement is done by monitoring the ratio of the relative intensities of the *trans-perp* HOONO to *cis-cis* HOONO overtone bands as a function of the flow cell residence time. The slope of each line is the decay rate in per second.

TABLE I. Molecular constants for the *cis-cis*, *trans-perp*, and *perp-perp* conformers of HOONO computed at the CCSD(T)/cc-pVTZ level, except for energies, which are reported at both the CCSD(T)/cc-pVTZ and CCSD(T)/cc-pVQZ//CCSD(T)/cc-pVTZ levels, relative to the *cis-cis* HOONO energy at each level of theory.

Geometries[a]	*Cis-cis* HOONO	*Trans-perp* HOONO	*Anti-perp-perp* HOONO
R(HO1) (Å)	0.9823	0.9663	0.9662
R(O1O2)	1.4332	1.4314	1.4384
R(O2N)	1.3845	1.4681	1.6070
R(NO3)	1.1917	1.1692	1.1512
θ(HO1O2)	99.80°	100.75°	100.57°
θ(O1O2N)	112.98°	105.50°	100.33°
θ(O2NO3)	114.39°	108.75°	109.74°
ϕ(HO1O2N)	0°	176.83°	82.65°
ϕ(O1O2NO3)	0°	97.59°	97.00°
A (MHz)	213 10	541 27	247 82
B	8081	4977	5896
C	5859	4627	5326
Energetics[b]			
CCSD(T)/cc-pVTZ			
E_{el} (hartrees)	−280.473 651 5	−280.467 470 7	−280.450 380 6
ΔE_{el} (kJ/mol)	0	16.2	61.1
ΔE_0 (kJ/mol)	0	14.6	56.9
ΔH°_{298} (kJ/mol)	0	15.9	57.0
CCSD(T)/cc-pVQZ//CCSD(T)/cc-pVTZ			
E_{el} (hartrees)	−280.560 370 6	−280.554 419 3	−280.537 308 1
ΔE_{el} (kJ/mol)	0	15.6	60.5
ΔE_0 (kJ/mol)	0	13.7	56.1
ΔH°_{298} (kJ/mol)	0	15.3	56.4
Harmonic frequencies[c] (cm^{-1})			
ν_1	3521 (a')	3780	3774
ν_2	1630 (a')	1736	1794
ν_3	1458 (a')	1412	1374
ν_4	969 (a')	992	906
ν_5	838 (a')	816	702
ν_6	723 (a')	497	468
ν_7	419 (a')	366	384
ν_8	523 (a'')	302	288
ν_9	383 (a'')	211	233*i*

[a]Atom labels are assigned as HO1O2NO3.
[b]Zero point and enthalpy corrections to E_{el} are determined from CCSD(T)/cc-pVTZ frequencies.
[c]Vibrational frequencies of *cis-cis* and *trans-perp* HOONO from Bean *et al.*, Ref. 9.

the 6971 cm^{-1} *trans-perp* HOONO feature at room temperature, and decays much more slowly than *trans-perp* HOONO does at colder temperatures. We therefore assign all of the bands in the room temperature spectrum to the lowest-energy conformer, *cis-cis* HOONO.

A 3 cm^{-1} resolution action spectrum of the 6365 cm^{-1} *cis-cis* HOONO band is shown in Fig. 5(b) along with a rotational band shape simulation from the ASYROTWIN program.[23] The upper and lower state rotational constants are taken from Table I, and a *b*-type band is assumed, based on calculations in Sec. IV D. The simulated *cis-cis* HOONO band has the pronounced *P* and *R* bands of a *b*-type transition, and is slightly broader than the *trans-perp* HOONO band, but the experimentally measured *cis-cis* HOONO band is significantly broader than predicted and has no resolvable structure. We conclude that some dynamical process, either IVR (intramolecular vibrational redistribution) or dissociation, is leading to the broadening and absence of rotational structure.

The *cis-cis* HOONO spectrum becomes progressively weaker at lower temperatures, most likely due to rapid wall loss. To observe the temperature dependence of the *cis-cis* HOONO spectrum over a larger temperature range, we employ an alternate synthesis of HOONO which does not require discharge chemistry (eliminating the need for long reaction times in the flow cell) and produces no detectable amount of *trans-perp* HOONO. HOONO is prepared by reacting H_2O_2 vapor with solid $NOBF_4$ *in situ*, analogous to the production of HO_2NO_2 from NO_2BF_4 described in Ref. 24. Using this preparation method, we observe no temperature dependence of the relative peak intensities in the *cis-cis* HOONO spectrum in the range 193–273 K (Fig. 9).

Weaker new bands are observed in the discharge HOONO synthesis at 6250 and 7700 cm^{-1} (Fig. 3). The peak at 6250 cm^{-1} is only observed at cold temperatures, coincident with the *trans-perp* HOONO peak at 6971 cm^{-1}, and is hence assigned to *trans-perp* HOONO. The temperature dependence of the 7700 cm^{-1} band was not studied systematically, therefore, this band cannot be assigned to either *trans-perp* or *cis-cis* HOONO.

B. OH product state distributions

The large differences in the structure and binding energy of *cis-cis* and *trans-perp* HOONO suggest that these two conformers should have distinct vibrational predissociation dynamics. The dynamical differences in the quantum state distribution of OH photofragments can be used to assist in spectroscopic assignment of various HOONO bands and provide other useful information. Pollack *et al.* analyzed the OH state distribution from the photolysis of supersonically cooled HOONO in the 6971 cm^{-1} band to constrain its binding energy to $D_0 < 70.3$ kJ/mol, consistent with an assignment of the band to the *trans-perp*, but not *cis-cis*, conformer of HOONO.[17]

In our experiment, the nascent energy distribution of the product OH fragments can be estimated by scanning over various OH lines with the LIF probe laser while the pump laser is fixed on a chosen OH overtone resonance of one of the HOONO conformers. To minimize thermalization of the OH prior to detection, the cell pressure and the pump-probe delay must be kept at their lowest possible values. The minimal pump-probe delay in this experiment is 50 ns, limited primarily by jitter in the pump-probe separation (10 ns) and by temporal width of the UV probe laser pulse (20 ns). In Ar bath gas, the average rotational energy transfer rate constant for $OH\,^2\Pi_{3/2}(v''=0)$, in $N''=1-5$, is $2.3 \times 10^{-11}\,cm^3\,molecule^{-1}\,sec^{-1}$.[25] At a pressure of 13 hPa, this corresponds to ~0.5 effective collisions between pump and probe pulses.

Despite this partial thermalization, a significantly different energy distribution in the OH photofragments is observed for the *cis-cis* and *trans-perp* conformers of HOONO. Figure 6 shows the observed distributions within the corresponding $^2\Pi^-_{3/2}(N)$ rotational manifolds obtained from analysis of $Q_{11}(N)$ branch of the $A\,^2\Sigma(v=1) \leftarrow X\,^2\Pi(v=0)$ band. The OH fragments from the photodissociation of *trans-perp* HOONO are rotationally excited, while the OH fragments from *cis-cis* HOONO are concentrated more heavily in the lowest *N* states, even though the *cis-cis* HOONO spectrum is recorded at a higher temperature. This distribution is consistent with the larger energy release $(h\nu - D_0)$ expected for *trans-perp* than for *cis-cis* HOONO based on the laser excitation energy and the empirically determined dissociation energies, providing further evidence that the transient feature observed is *trans-perp* HOONO.

C. *Trans-perp* to *cis-cis* HOONO isomerization rate

Flow cell kinetics experiments have been employed to measure the lifetime of *trans-perp* HOONO. At low temperatures, the signal from both conformers decays with residence time (distance from injector), but the *trans-perp* HOONO signal at 6971 cm^{-1} decays faster. The loss of *cis-cis* HOONO only occurs at temperatures below about 270 K, and the loss rate increases with decreasing temperature. We therefore conclude that the *cis-cis* HOONO decay is due to diffusion to the walls and subsequent uptake or reaction, while the faster decay of the *trans-perp* HOONO signal is due to isomerization. If we assume that both conformers of HOONO have the same wall loss rates in the flow cell, then the ratio of the *trans-perp* to *cis-cis* HOONO signals gives the *trans-perp* HOONO decay due to isomerization alone.

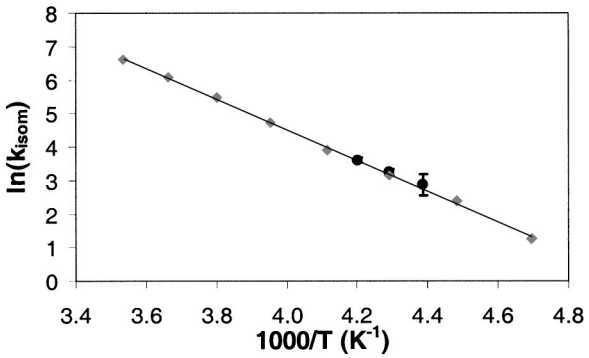

FIG. 8. *Trans-perp* to *cis-cis* HOONO isomerization rate as a function of temperature. Gray diamonds represent the results of a MULTIWELL simulation with an isomerization barrier of 40.8 kJ/mol at 8.7 hPa. Black circles are experimental data. Fit to the experimental data gives an isomerization activation barrier of E_{act} (230 K) = 33 ± 12 kJ/mol.

The relative ratio of intensities I_{tp}/I_{cc} of *trans-perp* to *cis-cis* HOONO signal is monitored at a series of injector positions (residence times) in the flow cell at several temperatures by measurement of signal intensity *I* at three wavelengths: one where both *trans-perp* and *cis-cis* HOONO absorb (6971 cm^{-1}), one which determines the baseline absorption by *cis-cis* HOONO underneath the 6971 cm^{-1} signal (6950 cm^{-1}), and one where only *cis-cis* HOONO signal is present (6365 cm^{-1}):

$$\frac{I_{tp}}{I_{cc}} = \frac{I(6971\ cm^{-1}) - I(6950\ cm^{-1})}{I(6935\ cm^{-1})}. \tag{3}$$

In addition, we assume that the increase in *cis-cis* HOONO signal due to the isomerization is negligible, since the number density of *trans-perp* HOONO is significantly lower than that of *cis-cis* HOONO, and since the spectrum is spread over a broad 1000 cm^{-1} wavelength range compared to the spectrally narrow 30 cm^{-1} *trans-perp* peak. A plot of $\ln(I_{tp}/I_{cc})$ versus residence time has a slope that is the unimolecular rate of *trans-perp* to *cis-cis* isomerization. Temperature-dependent isomerization rates are shown in Fig. 7, in the range $223 < T < 238$ K.

The lifetimes of *trans-perp* HOONO at 238, 233, and 228 K are estimated to be 27 ± 4, 39 ± 3, and 56 ± 6 ms, respectively, at 13 hPa of predominantly Ar. Unfortunately, we cannot probe the isomerization over a broader temperature range, because only one conformer can be detected with sufficient precision at colder and warmer temperatures. The data at 223 K show a very small slope and significant error; no accurate lifetime can be determined. The Arrhenius ln(*k*) versus 1/*T* relationship (Fig. 8) gives an activation energy for isomerization of $E_{act} \sim 33 \pm 12 (1\sigma)$ kJ/mol. The large uncertainty stems from the narrow temperature range used to determine E_{act}.

IV. COMPUTATIONAL RESULTS

A. *Ab initio* calculations of *cis-cis, trans-perp*, and *perp-perp* HOONO structures, energetics, and frequencies

The structures, energies, and vibrational frequencies of the *cis-cis*, *trans-perp*, and (*anti*-)*perp-perp* HOONO conformers have been calculated by electronic structure theory using the program GAUSSIAN 98.[26] For these calculations we use coupled cluster theory[27] with single and double excitations, with perturbative estimates of connected triples CCSD(T). The calculations employ the Dunning correlation consistent polarized valence basis sets. The two basis sets used in this study are the cc-pVTZ basis set ($4s3p2d1f$ for C, N, and O; $3s2p1d$ for H) and the cc-pVQZ basis set ($5s4p3d2f1g$ for C, N, and O; $4s3p2d1f$ for H).[28,29]

Optimized structures and vibrational frequencies of the three isomers are computed at the CCSD(T)/cc-pVTZ level. The *perp-perp* isomer possesses one imaginary frequency, corresponding to torsion of the heavy atoms (OONO). Energies at these geometries are computed at the CCSD(T)/cc-pVTZ and CCSD(T)/cc-pVQZ levels. Table I lists the structures, energies, rotational constants, and vibrational frequencies of the three conformers, with *perp-perp* HOONO computed in the *anti* configuration. The normal modes of the *trans-perp* and the *perp-perp* isomer are ordered in descending frequency, while the modes of the *cis-cis* isomer, which has C_s symmetry, are first ordered based on the symmetry, a' and then a''. The CCSD(T)/cc-pVQZ//CCSD(T)/cc-pVTZ energies are consistent with QCISD and CCSD(T)/cc-pVTZ results reported previously.[9]

B. Statistical (RRKM) calculations of isomerization rate

To better understand the observed temperature dependence of the HOONO action spectrum, we model the isomerization rates of HOONO conformers using the program MULTIWELL (version 1.3.3),[30] which uses a stochastic approach to solve RRKM master equations. The main goal of these simulations is to confirm that the experimentally determined rates of isomerization from the *trans-perp* conformer to the lower-energy *cis-cis* conformer are consistent with the *ab initio* energetics of HOONO. We adopt the required RRKM parameters from the model developed by Golden, Barker and Lohr,[2] which successfully reproduced the extensive kinetic data on the $OH+NO_2$ reaction (Hippler, Nasterlack and Striebel,[3] and others). The dissociation energy of *cis-cis* HOONO is fixed at 83 kJ/mol and the energy separation between *trans-perp* and *cis-cis* conformers is set to 15 kJ/mol. The average internal energy transferred per collision is chosen to be $\alpha=500$ cm^{-1}. The height of the *trans-perp*→*cis-cis* HOONO isomerization barrier (treated as a single transition state energy for both *perp-perp* states) is varied to reproduce the experimentally observed *trans-perp* isomerization rates. Because the reaction is in the low pressure limit, isomerization rates and collision parameter α are linearly related, and the *trans-perp*→*cis-cis* HOONO isomerization barrier determined is inversely correlated to the choice of $\alpha=500$ cm^{-1}. The simulation starts with the *trans-perp* conformer in an internally thermalized state, from which it can either reversibly isomerize into the *cis-cis* well or irreversibly dissociate into OH and NO_2. For the range of probed barrier heights (15–55 kJ/mol), the rate of dissociation into OH and NO_2 is negligibly small compared to the rate of equilibration between *cis-cis* and *trans-perp* conformers of HOONO. Therefore, the simulated time dependence for the *trans-perp* concentration can be directly fitted to an exponential decay to extract the effective equilibration rate ($=k_{tp\rightarrow cc}+k_{cc\rightarrow tp}\approx k_{tp\rightarrow cc}$).

The RRKM simulations of *trans-perp* to *cis-cis* HOONO isomerization presented here were performed assuming a bath gas of N_2. Our experimental gas mixture, however, consists of small amounts of H_2 and NO_2, 72% Ar, 14% He, and 12% N_2. Donahue *et al.*[31] have shown that relative to a collisional efficiency of $\beta=1$ for nitrogen, $\beta(\mathrm{Ar})=0.61\pm0.03$ and $\beta(\mathrm{He})=0.48\pm0.03$, in the $OH+NO_2$ system. For the gas mixture used in these experiments, then, the collisional efficiency is $\beta\approx0.65$. In the low pressure limit, which is applicable to these experiments at 13 hPa, this lower collision efficiency is equivalent to a lower pressure. Our gas mixture at 13 hPa behaves equivalently to pure N_2 at 8.7 hPa.

Figure 8 displays the calculated $k_{tp\rightarrow cc}$ isomerization rates at 8.7 hPa of N_2 as a function of temperature. The calculation uses the *trans-perp*→*cis-cis* HOONO isomerization barrier of $\Delta E_0=40.8$ kJ/mol (corresponding to an energy of $\Delta E_0=55.8$ kJ/mol for the *perp-perp* isomer relative to the *cis-cis* HOONO energy). The modeled *trans-perp* to *cis-cis* HOONO barrier height is in excellent agreement with the energy computed here at the CCSD(T)/cc-pVQZ//CCSD(T)/cc-pVTZ level, $\Delta E_0=42.4$ kJ/mol, and is also consistent with the energy computed by Golden, Barker, and Lohr[2] at the QCISD(T)/cc-pVDZ level (double ζ), 45.3 kJ/mol, for *perp-perp* HOONO relative to *trans-perp* HOONO.

The predicted temperature dependence of the isomerization rates compares favorably with the experimental results (black points in Fig. 8, derived from Fig. 7). The value suggested by our MULTIWELL simulations (40.8 kJ/mol) is within the error limits of the experimentally determined activation energy ($E_{act}=33\pm12$ kJ/mol).

C. Calculated photodissocation quantum yields and temperature dependence of relative band intensities in *cis-cis* HOONO

We also use MULTIWELL to predict the effective photodissociation quantum yields for the overtone transitions of *cis-cis* HOONO. The results of these simulations are shown in Figs. 9(a) and 9(b). In these simulations, the internal energy distribution for thermalized *cis-cis* HOONO is abruptly shifted upward by the photon energy. The fraction of HOONO conformers and $OH+NO_2$ products formed after 100 collisions following the excitation is taken as the yield. We use $D_0(cis\text{-}cis\ \mathrm{HO\text{-}ONO})=83$ kJ/mol (6940 cm^{-1}), which represents the best *ab initio* estimate from Dixon *et al.*[10] as well as the empirical value determined by extrapolation to 0 K from high-temperature data from Hippler, Nasterlack, and Striebel.[3]

Figure 9(a) depicts the fraction of *cis-cis* and *trans-perp* HOONO as well as $OH+NO_2$ produced as a function of

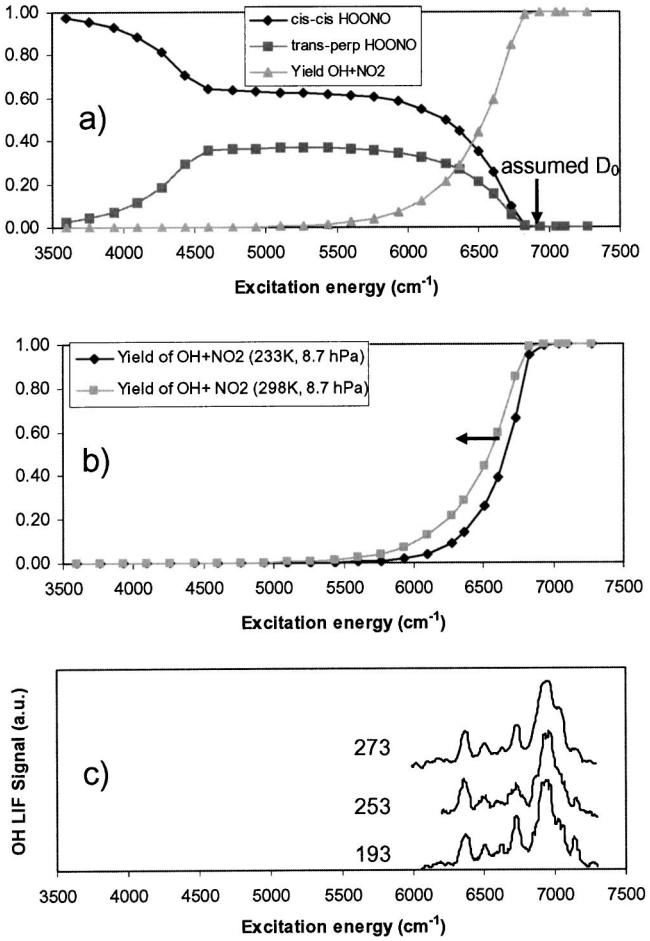

FIG. 9. Simulation of the quantum yield of *cis-cis* HOONO, *trans-perp* HOONO, and $OH+NO_2$ products, following vibrational excitation of *cis-cis* HOONO at 298 K as a function of excitation energy. Calculations assume a dissociation energy of $D_0(cis\text{-}cis\ \text{HOONO}) = 83$ kJ/mol (6940 cm^{-1}, shown with arrow). A significant yield of *trans-perp* HOONO is predicted after excitation above the isomerization barrier. The onset of dissociation occurs at 5500 cm^{-1}, well below the dissociation threshold. Calculations are run at 8.7 hPa N_2 (equivalent to 13 hPa of the gas mixture used in the above experiments, see text). (b) Photodissociation quantum yield as a function of excitation energy, calculated at 233 and 298 K, with $D_0(cis\text{-}cis\ \text{HOONO}) = 83$ kJ/mol. The quantum yield at the 6365 cm^{-1} peak is predicted to double when the temperature is changed from 233 to 298 K. (c) Experimentally measured *cis-cis* HOONO spectrum at three temperatures. The relative strengths of the bands in the *cis-cis* HOONO spectrum do not change appreciably over the temperature range 193–273 K.

energy added to the system at 298 K. When the system is excited above the isomerization barrier between 4500 and 6000 cm^{-1}, a significant amount of the original *cis-cis* HOONO isomerizes, forming a sizable fraction of *trans-perp* HOONO products as determined by the density of states at the isomerization barrier energy. Photodissociation products begin to appear at 5500 cm^{-1}, with the yield slowly rising to ~50% at 6600 cm^{-1} (still well below D_0). The quantum yield is predicted to approach unity at 6700 cm^{-1}.

Figure 9(b) compares the $OH+NO_2$ yield for two temperatures representative of our experimental conditions. Over the frequency range of the observed *cis-cis* HOONO spectrum, we find that the quantum yield for photodissociation increases from 30% to 100% at 298 K and from 15% to 100% at 233 K. At the 6365 cm^{-1} peak, the quantum yield is predicted to double from 233 to 298 K. Thus, the simulations predict that the relative intensities of the bands should change markedly as a function of temperature.

Figure 9(c) shows the positions of the *cis-cis* HOONO bands on the scale of the quantum yield predictions, and also illustrates the insensitivity of the spectrum to temperature change. We observe no discernable change in relative integrated peak intensities in the *cis-cis* HOONO spectrum over the range 193–273 K.

D. Calculated transition strengths of *cis-cis* and *trans-perp* HOONO

To estimate the relative concentrations of the *cis-cis* and *trans-perp* HOONO from the observed band intensities, we perform semiempirical calculations to compute transition strengths for the observed overtone bands of both isomers. We test the validity of our normal mode anharmonic oscillator and Morse oscillator approaches by calculating band intensities of the ν_1 and $2\nu_1$ transition of nitric acid, for which experimentally determined oscillator strengths and further predictions are available.

The method of using *ab initio* dipole moment functions in calculating vibrational band intensities has been demonstrated.[32,33] Vibrational band intensity calculations similar to those reported here have been performed by Kjaergaard, Henry, and others on several molecules using a local mode harmonically coupled anharmonic oscillator model[34–36] and coupled Morse oscillators.[37] For calculation of the OH fundamental and overtone in HOONO described here, we consider only the OH normal mode.

The oscillator strength for a given vibrational transition is given by

$$f_{fi} = \frac{4\pi m_e}{3e^2\hbar}\nu_{fi}\sum_{i=a,b,c}|M_i|^2, \tag{4}$$

where ν_{fi} is the frequency of the transition and M_i are the matrix elements of the transition dipole moment between the ground and excited vibrational states:

$$M_i = \langle f|\mu_i|i\rangle. \tag{5}$$

The values of the matrix elements M_i for the $v = 0 \rightarrow 2$ overtone transitions are obtained by first computing *ab initio* dipole moment functions along one dimension, the normal mode q_1 (essentially the OH stretch). The vibrational matrix elements are then calculated using two different one-dimensional models, an anharmonic oscillator model with a single cubic perturbation, and the Morse oscillator model, where the parameters for both models are fit using observed vibrational energies.

Dipole moment functions are calculated for both *cis-cis* and *trans-perp* HOONO structures using the GAUSSIAN98 program.[26] Optimized structures for each isomer are first determined at the B3LYP/AUG-cc-pVTZ, MP2/AUG-cc-pVTZ, MP3/AUG-cc-pVDZ, and QCISD/AUG-cc-pVDZ levels of theory (where AUG denotes diffuse function augmented basis sets). The atoms are then displaced in 0.1 $amu^{1/2}$ Å increments (Note: GAUSSIAN 98 normal mode outputs are in Cartesian coordinates. Conversion to $amu^{1/2}$ Å

TABLE II. Computed dipole moment functions in Debye for *trans-perp* and *cis-cis* conformers of HOONO as a function of normal mode displacement q_1. Taylor series coefficients were derived from the fitting of a fifth-order polynomial (see text) to *ab initio* dipole moments at nine points along the q_1 normal mode, computed in 0.1 amu$^{1/2}$ Å increments in the range $-0.4\,\text{amu}^{1/2}\,\text{Å} < \Delta q_1 < +0.4\,\text{amu}^{1/2}\,\text{Å}$. Coefficients are defined as $c_{i,n} = (1/n!)(\partial^n \mu_i / \partial q_1^n)$, where $i = A, B, C$, the principal axes. Units are D amu$^{-n/2}$ Å^{-n}.

	B3LYP AUG-cc-pVTZ	MP2 AUG-cc-pVTZ	MP3 AUG-cc-pVDZ	QCISD AUG-cc-pVDZ
Trans-perp HOONO				
Reduced mass (amu)	1.0686	1.0686	1.0684	1.0685
$\lvert\mu_{\text{tot}}\rvert$ (equil)	1.7330	1.8758	2.0498	1.9724
$\mu_{0,A}$	0.7470	0.6909	1.0488	0.8562
$c_{A,1}$	0.8067	0.9256	0.8837	0.9043
$c_{A,2}$	−0.6961	−0.8855	−0.8046	−0.8230
$c_{A,3}$	−2.6773	−0.3270	−0.2301	−0.2139
$c_{A,4}$	−5.5369	0.0499	−0.0640	−0.0526
$c_{A,5}$	14.9472	0.5069	0.7197	0.6901
$\mu_{0,B}$	−0.3478	−0.6010	−0.5989	−0.6306
$c_{B,1}$	−0.0320	−0.0569	−0.1604	−0.1009
$c_{B,2}$	0.4737	0.2048	0.1460	0.1860
$c_{B,3}$	−0.1344	−0.0882	−0.1097	−0.1006
$c_{B,4}$	−1.9665	−0.0123	−0.0001	0.0150
$c_{B,5}$	0.5710	−0.0568	−0.2200	−0.1946
$\mu_{0,C}$	1.5310	1.6370	1.6557	1.6609
$c_{C,1}$	0.8302	1.1023	1.1150	1.1205
$c_{C,2}$	−0.5782	−0.2726	−0.2353	−0.2249
$c_{C,3}$	−1.1973	−0.7564	−0.7030	−0.6433
$c_{C,4}$	−0.6951	0.1149	0.2032	0.2490
$c_{C,5}$	0.6047	0.5634	0.4862	0.2819
Cis-cis HOONO				
Reduced mass (amu)	1.0643	1.0640	1.0642	1.0641
$\lvert\mu_{\text{tot}}\rvert$ (equil)	0.9618	1.1744	1.1987	1.2276
$\mu_{0,A}$	−0.4042	−0.7435	−0.7513	−0.8604
$c_{A,1}$	−0.5378	−0.7808	−0.7929	−0.8628
$c_{A,2}$	−3.4439	−1.1959	−1.2353	−1.3039
$c_{A,3}$	3.4255	−0.2171	−0.1870	−0.2322
$c_{A,4}$	14.5912	0.0450	−0.1166	−0.0649
$c_{A,5}$	−28.5687	0.2815	0.3832	0.4338
$\mu_{0,B}$	−0.9096	−0.9090	−0.9337	−0.8753
$c_{B,1}$	−0.4418	−1.1157	−1.0871	−1.0676
$c_{B,2}$	−1.3162	−0.0838	−0.0801	−0.0926
$c_{B,3}$	−2.9383	−0.3229	−0.3965	−0.4281
$c_{B,4}$	12.6755	−0.2311	−0.1332	−0.1372
$c_{B,5}$	−2.8530	−0.2012	−0.3487	−0.3588
$\mu_{0,C}$	0	0	0	0
$c_{C,1}$	0	0	0	0
$c_{C,2}$	0	0	0	0
$c_{C,3}$	0	0	0	0
$c_{C,4}$	0	0	0	0
$c_{C,5}$	0	0	0	0

units, and conversion of dipole derivatives to D amu$^{n/2}$ Å^{-n} units, was done after calculation.) from the optimized geometries along the q_1 normal mode to generate nine structures along the vibrational mode ($+0.4\,\text{amu}^{1/2}\,\text{Å} > \Delta q_1 > -0.4$ amu$^{1/2}$ Å). This normal mode displacement involves primarily motion of the H atom along the OH bond, with small concomitant motion of the adjacent O atom. The dipole moments are computed for each of these nine structures, for each principal axis component (i), at each level of theory. These points are then fit to a Taylor series expansion, truncated after the fifth derivative, to extract the derivatives of the dipole moment function used in the transition moment calculation:

$$\mu_i = \mu_{0,i} + \sum_{n=1}^{5} \frac{1}{n!} \frac{\partial^n \mu_i}{\partial q^n} q^n = \mu_{0,i} + \sum_{n=1}^{n} c_{i,n} q^n. \tag{6}$$

Table II lists $\mu_{0,i}$ and coefficients $c_{i,n}$ at all levels of theory used. Also listed is μ_1, the effective reduced mass of the mode q_1, computed in the GAUSSIAN 98 program at each level of the theory.[38,39]

We have found that the dipole moment function predicted by the hybrid density functional theory (DFT) B3LYP method does not vary smoothly with q_1. Thus, DFT does not seem to be adequate for calculating the dipole moments of HOONO. The erratic variations in electric moment is evi-

TABLE III. Observed vibrational bands, and fitted harmonic frequencies and anharmonicities (cm^{-1}) for the stable conformers of HOONO.

	ν_1	$2\nu_1$	ω_e	$\omega_e x_e$
Cis-cis HOONO	3306[a]	6365[b]	3548	121
Trans-perp HOONO	3574[c]	6971[d]	3751	88.5

[a]Reference 9.
[b]Reference 11 and this work.
[c]Based on *ab initio* frequency, Ref. 9, and matrix isolation spectrum, Ref. 19.
[d]Reference 17 and this work.

dence of orbital switching and/or configuration mixing in HOONO, which suggests that a single configuration method is inadequate to describe the wave functions of either conformer of HOONO. While the DFT method has been reported to predict dipole moment functions for molecules such as H_2O that can be accurately described by a single configuration,[40] it does not seem to predict accurate dipole moments functions for HOONO, particularly in the hydrogen-bonded *cis-cis* conformer. Kjaergaard *et al.* have observed the same inadequacy of DFT in determination of electrostatic moments in systems with hydrogen bonding in the case of the water dimer.[41]

Our *ab initio* calculations predict that *trans-perp* HOONO has a larger permanent dipole moment than *cis-cis* HOONO, and one that points predominantly along the *c* axis of the molecule. The permanent dipole moment in *cis-cis* HOONO roughly bisects the *a* and *b* axes in the plane of the molecule and points towards the terminal O with a slightly larger component along the *b* axis than the *a* axis. These principal axes are shown in Fig. 1. The first derivatives of the dipole moment can be used to estimate the transition strength of the ν_1 fundamental band in the harmonic limit, and compared to transition strengths determined from analytical gradients computed at the equilibrium geometry. For both *trans-perp* and *cis-cis* HOONO, at the MP2/AUG-cc-pVTZ, MP3/AUG-cc-pVDZ, and QCISD/AUG-cc-pVDZ levels of theory, our numerical derivatives give transition strengths that are roughly a factor of 2 larger than those calculated from single-point analytic derivatives. This discrepancy suggests the degree to which the single-point methods diverge from an explicit calculation of the dipole moment function over a larger geometry change.

In the first approach to calculate transition strengths, we treat the OH normal mode as an anharmonic oscillator with a single cubic perturbation term, and obtain anharmonic wave functions by fitting the predicted energy levels (diagonalizing the Hamiltonian to $v=12$) to observed ν_1 and $2\nu_1$ band positions (Table III). The fundamental of *trans-perp* HOONO has not yet been observed in the gas phase, so we estimate it to be 3574 cm^{-1} from prior *ab initio* predictions,[15] which are consistent with the observed Ar matrix frequency.[19] The $2\nu_1$ transition moments are then obtained by numerical integration over the fitted dipole moment function and anharmonic initial and final state wave functions.

In the second approach, we calculate the overtone transition moments assuming the OH stretch could be modeled as a Morse oscillator fit to $\omega_e x_e$ and ω_e parameters derived from observed ν_1 and $2\nu_1$ band positions for *cis-cis* HOONO, and predicted ν_1 and observed $2\nu_1$ band positions for *trans-perp* HOONO. We use expressions for the Morse oscillator transition matrix elements of first, second, and third order given by Gallas.[42]

To examine the validity of these two methods, we compute the oscillator strengths for both the fundamental and first overtone of nitric acid, for which extensive experimental and computational results are available. We compute the dipole moment function for nitric acid at the MP2/AUG-cc-pVTZ level of theory over the same $+0.4\,\mathrm{amu}^{1/2}\,\text{Å} > \Delta q_1 > -0.4\,\mathrm{amu}^{1/2}\,\text{Å}$ range.

For the fundamental ν_1 OH transition in nitric acid, Lange *et al.*[43] find an oscillator strength of $f_{10}=1.07\times10^{-5}$ ($\tilde{\sigma}_{10}=9.46\times10^{-18}\,\mathrm{cm}^2/\mathrm{molecule\,cm}$), while Chackerian, Sharpe, and Blake[44] obtain $f_{10}=1.40\times10^{-5}$ ($\tilde{\sigma}_{10}=1.24\times10^{-17}\,\mathrm{cm}^2/\mathrm{molecule\,cm}$). Our anharmonic oscillator method gives $f_{10}=2.60\times10^{-5}$, while the Morse oscillator method gives $f_{10}=5.06\times10^{-5}$. A recent single-point *ab initio* prediction[9] of the OH fundamental intensity in the double harmonic approximation yielded $f_{10}=1.69\times10^{-5}$ (90 km/mol).

The oscillator strength of the first overtone band of nitric acid is also known experimentally and has been calculated previously. The experimental oscillator strength is $f_{20}=3.75\times10^{-7}$ ($\tilde{\sigma}_{20}=3.32\times10^{-19}\,\mathrm{cm}^2/\mathrm{molecule\,cm}$), as determined by Lange *et al.*[43] The oscillator strength calculated by the anharmonic oscillator method presented here is $f_{20}=2.26\times10^{-7}$, while the prediction from the Morse oscillator method is $f_{20}=4.49\times10^{-7}$. Other *ab initio* techniques predicted yet higher oscillator strengths for the first overtone of nitric acid. Donaldson *et al.*[45] compute $f_{20}=5.96\times10^{-7}$ at the QCISD/6-31+G(d,p) level (unscaled). Rong *et al.* calculate $f_{20}=7.11\times10^{-7}$ at the QCISD/6-311++G($2d$,$2p$) level using an empirical Deng-Fan potential, and $f_{20}=6.05\times10^{-7}$ using a Morse oscillator approach.[46]

The results of both the anharmonic and Morse oscillator approaches for HOONO are given in Table IV. The difference in the anharmonic and Morse oscillator results indicate the accuracy of modeling transitions in the lowest vibrational levels. We note that this simple treatment does well at these low vibrational levels. The relative transition strengths of *cis-cis* to *trans-perp* HOONO $2\nu_1$ bands for both methods and all four levels of theory used are listed in Table V. In all cases, the B3LYP method does not give reliable single-point dipole moments for HOONO, and the resulting transition dipole matrix elements and oscillator strengths deviate significantly from the MP2 and higher level results. We therefore do not use the B3LYP results to compute transition strengths. Both the anharmonic oscillator and the Morse oscillator method predict a stronger $2\nu_1$ transition for *trans-perp* than for *cis-cis* HOONO, by a factor of 3.7:1 and 3.2:1, respectively, at the QCISD/AUG-cc-pVDZ level. The methods agree reasonably well, with the Morse oscillator method predicting consistently higher transition dipole moments and oscillator strengths.

The QCISD level anharmonic oscillator calculation predicts that the $2\nu_1$ spectrum of *trans-perp* HOONO should be

TABLE IV. Calculated values of the transition dipole moment matrix elements M_i, oscillator strengths f, and rovibrational hybrid band types for the $2\nu_1$ overtone transitions of *trans-perp* and *cis-cis* HOONO. Matrix elements were computed by integrating *ab initio* dipole moment functions using both anharmonic oscillator and Morse oscillator methods. Units of M_A, M_B, and M_C are Debye; units of $|M_{\text{tot}}|^2$ are Debye^2.

	B3LYP AUG-cc-pVTZ	MP2 AUG-cc-pVTZ	MP3 AUG-cc-pVDZ	QCISD AUG-cc-pVDZ
Trans-perp HOONO				
Anharmonic oscillator				
M_A	-1.07×10^{-2}	-1.08×10^{-2}	-1.00×10^{-2}	-1.02×10^{-2}
M_B	2.72×10^{-3}	1.57×10^{-3}	1.75×10^{-3}	1.68×10^{-3}
M_C	-8.84×10^{-3}	-8.01×10^{-3}	-7.80×10^{-3}	-7.77×10^{-3}
$\lvert M_{\text{tot}}\rvert^2$	2.01×10^{-4}	1.82×10^{-4}	1.64×10^{-4}	1.67×10^{-4}
f	6.59×10^{-7}	5.98×10^{-7}	5.37×10^{-7}	5.48×10^{-7}
Hybrid band *a*-type to *c*-type ratio	1.5:1	1.8:1	1.7:1	1.8:1
Morse oscillator method				
M_A	-1.19×10^{-2}	-1.25×10^{-2}	-1.16×10^{-2}	-1.19×10^{-2}
M_B	3.01×10^{-3}	1.61×10^{-3}	2.02×10^{-3}	1.82×10^{-3}
M_C	-1.04×10^{-2}	-1.04×10^{-2}	-1.02×10^{-2}	-1.02×10^{-2}
$\lvert M_{\text{tot}}\rvert^2$	2.58×10^{-4}	2.66×10^{-4}	2.44×10^{-4}	2.48×10^{-4}
f	8.46×10^{-7}	8.73×10^{-7}	8.00×10^{-7}	8.14×10^{-7}
Hybrid band *a*-type to *c*-type ratio	1.3:1	1.4:1	1.3:1	1.4:1
Cis-cis HOONO				
Anharmonic oscillator				
M_A	-1.48×10^{-2}	-2.79×10^{-3}	-3.04×10^{-3}	-2.99×10^{-3}
M_B	-4.26×10^{-3}	6.78×10^{-3}	6.57×10^{-3}	6.36×10^{-3}
M_C	0	0	0	0
$\lvert M_{\text{tot}}\rvert^2$	2.36×10^{-4}	5.38×10^{-5}	5.24×10^{-5}	4.93×10^{-5}
f	7.07×10^{-7}	1.61×10^{-7}	1.57×10^{-7}	1.48×10^{-7}
Hybrid band *b*-type to *a*-type ratio	0.1:1	5.9:1	4.7:1	4.5:1
Morse oscillator method				
M_A	-1.34×10^{-2}	-1.52×10^{-4}	-3.18×10^{-4}	-5.50×10^{-5}
M_B	-6.24×10^{-3}	9.78×10^{-3}	9.47×10^{-3}	9.19×10^{-3}
M_C	0	0	0	0
$\lvert M_{\text{tot}}\rvert^2$	2.19×10^{-4}	9.56×10^{-5}	8.98×10^{-5}	8.44×10^{-5}
f	6.57×10^{-7}	2.86×10^{-7}	2.69×10^{-7}	2.53×10^{-7}
Hybrid band *b*-type to *a*-type ratio	0.2:1	*b*-type only	*b*-type only	*b*-type only

a hybrid band with a ratio 1.8:1 *a*-type to *c*-type. Figure 5(a) shows that a band contour simulation agrees very well with the experimental spectrum. This ratio also agrees with the approximate experimental ratio of 1:1 adopted by Pollack *et al.*[17] for the same transition. In the case of *cis-cis* HOONO, no structure is observed on the $2\nu_1$ band in this experiment, hence, there is no experimental test for the QCISD/AUG-cc-pVDZ calculated hybrid band *b*-type to *a*-type ratio of 4.5 to 1. Bean *et al.*[9] find that a range of ratios of *b*-type to *a*-type from 1 to 4 provide an acceptable fit to their cavity ring down spectrum of ν_1 (*cis-cis* HOONO). Our anharmonic method predicts a *b*-type to *a*-type ratio of 2 for

TABLE V. Ratio of $2\nu_1$ overtone oscillator strength for *trans-perp* vs *cis-cis* HOONO at each level of theory.

	Oscillator strength ratio (tp:cc ratio)			
	B3LYP/ AUG-cc-pVTZ	MP2/ AUG-cc-pVTZ	MP3/ AUG-cc-pVDZ	QCISD/ AUG-cc-pVDZ
Anharmonic oscillator method	0.9:1	3.7:1	3.4:1	3.7:1
Morse oscillator method	1.3:1	3.0:1	3.0:1	3.2:1

the fundamental OH stretch of *cis-cis* HOONO, consistent with the experimental bounds.

E. Relative populations of *cis-cis* and *trans-perp* HOONO

In principle, the initial populations of the two conformers of HOONO can be estimated using the computed oscillator strengths, if we assume that all long-lived peaks in the HOONO spectrum belong to *cis-cis* HOONO and derive their intensity from the $2\nu_1$ transition. At the earliest time in the flow cell at which HOONO can be observed, the ratio of the integrated area of the *cis-cis* conformer bands to that of the *trans-perp* bands is about 5:1 at 233 K. With the relative transition strength of *trans-perp* to *cis-cis* HOONO of 3.7:1 and assuming unit photodissociation quantum yield for both species, this leads to an approximate upper bound on the initial *cis-cis* to *trans-perp* HOONO concentration ratio of 19:1. This supports the assumption that no rise in *cis-cis* HOONO signal should be detectable due to isomerization, since $n_{tp} \ll n_{cc}$.

This estimate is only an upper bound on the true initial *cis-cis* to *trans-perp* HOONO concentration ratio, because there is a sizable delay between when reaction occurs and when HOONO concentrations are probed. As seen in Fig. 7, the shortest residence time is 80 ms, based on the estimated flow velocity and injector/laser-interaction region distance. This residence time is on the same order of magnitude as the observed isomerization lifetimes; thus, a significant fraction of *trans-perp* HOONO will have isomerized prior to the laser measurement. However, our estimate of residence time is qualitative. The injector flow velocity is significantly greater than the velocity of background NO_2/N_2 gas mixture entering the flow cell. Thus, it is possible that the formation of OH and subsequent reaction with NO_2 occurs over a range of distances from the injector inlet. This does not adversely impact our measured isomerization rates, since the *trans-perp* HOONO lifetime data show completely single exponential behavior.

V. DISCUSSION

A. Kinetics scheme for HOONO formation and isomerization

The experimental results and RRKM simulations reported here confirm the kinetics scheme for formation of HOONO shown in Fig. 10, developed by Golden, Barker, and Lohr.[2]

Collisional stabilization forms an initially energy-rich HOONO far above the *cis-cis*↔*trans-perp* HOONO isomerization barrier (but below the barrier for dissociation back into OH and NO_2). The isomerization rates between the two isomers are substantially faster than the collision rate at 13 hPa; thus the isomers are in microcanonical equilibrium with relative populations determined by the specific density of states. The two isomers remain in microcanonical equilibrium as they are collisionally relaxed, until the internal energy approaches the barrier height (the two nearly isoenergetic *perp-perp* isomers). Further collisions then relax HOONO below the isomerization barrier, and rapidly form

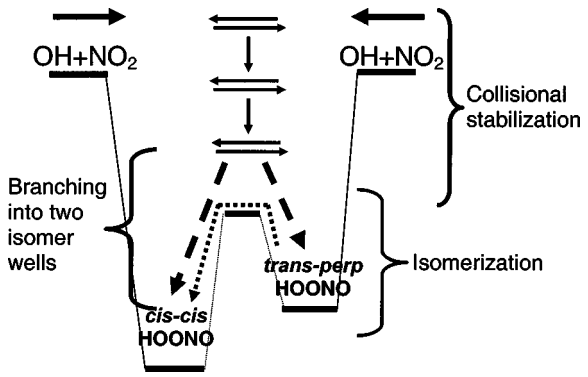

FIG. 10. Proposed kinetic scheme for $OH + NO_2 \rightarrow$ HOONO formation. The initially produced HOONO has enough internal energy for a facile isomerization between the *cis-cis* HOONO and *trans-perp* HOONO wells. After a few collisions, the system relaxes into the wells with a comparable yield of both conformers. Slow isomerization from the *trans-perp* HOONO into the *cis-cis* HOONO well then occurs on the millisecond time scale.

thermalized *cis-cis* and *trans-perp* isomers. This picture is illustrated by our RRKM simulation (Fig. 9), where we find that if HOONO is placed in either *cis-cis* or *trans-perp* HOONO well at any energy between isomerization and dissociation barriers, the system promptly relaxes below the isomerization barrier into both wells after just a few collisions (at $T = 230$ K and $P = 13$ hPa in N_2 buffer).

The initial ratio of the thermalized conformers formed is thus determined by the relative density of states of the two isomers at the *perp-perp* isomer barrier energy, which statistical modeling of the experimentally measured rates predicts to be 40.8 kJ/mol above the *trans-perp* energy. This ratio is predicted to be 2:1 *cis-cis* HOONO to *trans-perp* HOONO using the densities of states from Golden, Barker, and Lohr.[2] Thus, the initial population of *trans-perp* HOONO is substantially higher than expected from a Boltzmann distribution (<1%). The high relative abundance of the less stable *trans-perp* isomer arises because the *trans-perp* HOONO density of states rises more rapidly with energy than that of *cis-cis* HOONO. Our own 233 K estimate of this *cis-cis* to *trans-perp* HOONO ratio is 19:1, measured at a distance ~80 ms downstream from the discharge inlet in the flow cell. This result confirms that substantial population of *trans-perp* HOONO is formed at temperatures below 233 K.

This nonthermal population of *trans-perp* HOONO subsequently relaxes to *cis-cis* HOONO by isomerization. Our experiment shows that the HOONO population shifts to the *cis-cis* HOONO well (thermal equilibrium) within ~100 ms (at 13 hPa), consistent with RRKM modeling.

B. Spectral assignment of the *cis-cis* HOONO action spectrum

The room temperature HOONO action spectrum comprises several bands with no resolvable structure. The intensity pattern is also unusual, with the strongest band at 6935 cm^{-1}. Nizkorodov and Wennberg[11] tentatively assigned these bands to three conformers of HOONO: *cis-cis*, *cis-perp*, and *trans-perp* HOONO. We have found that *all* features in the spectrum observed above 240 K arise from the same conformer. We have also observed that *trans-perp* HOONO can-

not give rise to any of these features, since this conformer is observed only transiently at lower temperatures. Finally, recent calculations[2,10] indicate that *cis-perp* HOONO is not a stable isomer.

We therefore propose that these bands be assigned to the $2\nu_1$ overtone and $2\nu_1$-containing combination bands and/or sequence bands of *cis-cis* HOONO. Based on our observations and calculations, we suggest possible new assignments for the *cis-cis* HOONO action spectrum. It must be emphasized that these are tentative assignments.

We assign the first strong peak, at 6365 cm^{-1}, to the origin of the *cis-cis* HOONO overtone ($2\nu_1$). The position, 580 cm^{-1} lower in energy than the $2\nu_1$ origin of nitric acid, is in accord with our expectations for the overtone of the hydrogen-bonded OH stretch in *cis-cis* HOONO. Bean *et al.*[9] have observed that the band origin of the fundamental $1\nu_1$ band is redshifted by $\sim$250 cm^{-1} from the free OH stretch of nitric acid. The somewhat larger anharmonic correction, $\omega_e x_e = 121\ cm^{-1}$ (Table III), is expected with internal hydrogen bonding.

This 6365 cm^{-1} band is featureless and appears to be broadened significantly compared to the expected width of the rotational band contour [Fig. 5(b)]; the other bands in the room temperature spectrum have similar widths. In contrast, the observed band of the *trans-perp* isomer is well fit by the predicted rotational band contour. These observations indicate that the *cis-cis* conformer of HOONO must undergo relatively rapid IVR, leading to intrinsic line broadening beyond the width predicted on the basis of the predicted rotational band contour. The rapid IVR may be due to the presence of the intramolecular hydrogen bond in the *cis-cis* conformer, since hydrogen bonds greatly enhance coupling of the OH stretching vibration to the lower-frequency modes.

Computed frequencies provide some guidance in assigning the remaining bands. The highest level theoretical frequencies computed to date are shown in Table I. The four lowest-frequency modes for *cis-cis* HOONO are the two in-plane a' modes, the NO stretch (ν_6) and the NOO bend/intermolecular OH$\cdots$O stretch (ν_7), and the two out-of-plane a'' modes, the ONOO torsion (ν_8) and the HOON torsion (ν_9). Examination of the normal mode displacements indicates that the two torsional modes are thoroughly mixed. However, these are harmonic predictions of modes with large amplitude displacements and may have significant uncertainty.

One possible assignment relies on matching the observed band positions to the above *ab initio* frequencies. We then assign $2\nu_1+\nu_9$ to the 6730 cm^{-1} band, $2\nu_1+\nu_8$ to the broad 6935 cm^{-1} band, and $2\nu_1+\nu_6$ to the 7045 cm^{-1} band. Bands at 6180, 6505, and 6630 cm^{-1}, close to the pure $2\nu_1$ band, would then be assigned as torsional sequence bands of $2\nu_1$.

The difficulty with this assignment is the anomalous intensity pattern of the room temperature *cis-cis* HOONO spectrum. One normally expects the $2\nu_1$ origin to be the strongest band, since the OH stretch is the only expected bright state at this energy. However, the band at 6935 cm^{-1} is $\sim$three times stronger.

The most plausible explanation is that the action spectrum does not reproduce the absorption strengths, because the quantum yield for dissociation is not unity across this wavelength range. Our statistical calculations (Fig. 9) show that, if the dissociation energy of *cis-cis* HOONO is 83 kJ/mol (6940 cm^{-1}),[3] then the lower-frequency bands are suppressed due to nonunity quantum yield. At our assigned origin of the $2\nu_1$ transition frequency, 6365 cm^{-1}, only $\sim$30% of the *cis-cis* HOONO molecules will dissociate upon photon excitation at room temperature.

However, these calculations also predict that the quantum yield of the origin band will increase significantly (a factor of two) from 233 to 298 K, while we observe that all bands in this spectrum scale together over the temperature range 193–273 K.

It is possible that a coincidence of two effects leads to this observation. If the higher-energy band(s) around 6935 cm^{-1} are hot bands ($v>0$) which only have sufficient thermal population of the excited initial state to be observed at higher temperatures, then the intensity of these bands will decrease as the temperature is lowered. The lower-energy bands will decrease with lowering temperature due to the temperature dependence of the quantum yield, and if these two temperature effects coincide, no apparent change in relative band intensity would be observed.

It is also possible that the assumed 83 kJ/mol dissociation energy is too high. Lowering the dissociation energy in the model would simply shift the $OH+NO_2$ photodissociation yield curve down the frequency axis, and a shift of 5 kJ/mol [indicated by an arrow in Fig. 9(b)] would lead to near-unity quantum yield over all bands in the *cis-cis* HOONO spectrum and no temperature dependence of the relative peak intensities. This would give an experimental upper limit on the *cis-cis* HOONO bond dissociation energy of $D_0(cis\text{-}cis\ \text{HO-ONO}) \leqslant 78$ kJ/mol (6520 cm^{-1}).

If $D_0(cis\text{-}cis\ \text{HO-ONO}) \leqslant 78$ kJ/mol, the anomalously high intensity of the 6935 cm^{-1} band requires explanation. The intensity of this band may result from strong coupling of the OH stretch with other degrees of freedom, especially the OH torsional mode. The strength of this 6935 cm^{-1} band might be reasonable if it is a superposition of several combination bands of the form $2\nu_1+n\nu_9$, and the OH—torsion coupling is strong. Multidimensional potential and dipole surfaces, as demonstrated successfully for CH-stretching overtone spectra of methyl rotors,[47] would be required to fully analyze this coupling.

Our experimental evidence is not sufficient to determine the dissociation energy for *cis-cis* HOONO. Direct absorption measurements of *cis-cis* HOONO in the overtone energy regime are currently underway; these measurements would not be subject to quantum yield considerations, and would assist in assigning this spectrum.

C. Atmospheric implications

Isomerization of *trans-perp* to *cis-cis* HOONO occurs in milliseconds, even at low pressure. As a result, only the *cis-cis* conformer of HOONO will have appreciable concentration in Earth's atmosphere. In addition, the collisional isomerization rate is sufficiently fast that *trans-perp* HOONO will not be present at significant concentrations in

gas cell studies near room temperature. For example, Bean *et al.*[9] have reported cavity ring down spectroscopy (CRDS) of *cis-cis* HOONO, and determined a branching ratio of reaction (1a) and (1b). This branching ratio assumes that all HOONO is present in the *cis-cis* form on the 50–200 ms time scale of the CRDS experiment, since the HOONO yield is determined from the integrated *cis-cis* HOONO band. In CRDS, *trans-perp* HOONO signal would be buried in the extremely strong $HONO_2$ band, and hence difficult to discern. The fast *trans-perp* to *cis-cis* isomerization rates determined here support the assumption made by Bean *et al.* to derive the HOONO to $HONO_2$ branching ratio.

Our study allows estimation of the *cis-cis* HOONO lifetime in Earth's atmosphere. This lifetime is derived from a calculation similar to that used to predict the HO_2NO_2 near-IR photolysis lifetime.[48] Excitation of $2\nu_1$ and companion bands will be an efficient loss mechanism for HOONO. The average solar radiance at 1.4 μm is 4.90×10^{13} photons $cm^{-2}\,s^{-1}/cm^{-1}$.[49] The predicted oscillator strength of 1.5×10^{-7} gives an integrated band intensity for *cis-cis* HOONO of $1.3\times10^{-19}\,cm^2$ molecule cm^{-1}. Assuming unit quantum yield for photodissociation, the resulting photolysis rate of HOONO in the atmosphere due only to IR excitation will be $\sim6\times10^{-6}\,s^{-1}$, leading to an upper limit estimate for the *cis-cis* HOONO lifetime of 1.6×10^5 s (less than 45 daylight hours). Other losses (e.g., thermal decomposition, UV photolysis, and reaction with OH) will shorten this lifetime further. For example, using the kinetic parameters from Golden, Barker and Lohr,[2] we predict that HOONO thermal decomposition lifetimes range from a few seconds at the surface to 3.3×10^6 s (38 days) at the tropopause. Thermal decomposition is the dominant removal mechanism in the lower troposphere.

The short lifetime of HOONO suggests that its photochemistry will not be of major importance in Earth's atmosphere. Consider the polar lower stratosphere in summer—a region and time characterized by both fast gas-phase formation of HNO_3 and temperatures that are cold enough to yield a long HOONO thermal lifetime. At 20 km altitude, where [OH] concentrations are $\sim2\times10^6$ molecules cm^{-3} (1 pptv), the reaction of OH with NO_2 proceeds at a rate of $\sim1\times10^4$ molecules $cm^{-3}\,s^{-1}$.[50] Assuming a 10% yield of HOONO in this reaction and the maximum HOONO lifetime (1.6×10^5 s), the upper limit for the concentration of HOONO is 1.6×10^8 molecules cm^{-3}, or 80 pptv. This concentration of HOONO may be detectable via remote measurement in the IR or far-IR but we stress this is an upper limit and UV photolysis and reaction with OH will certainly lead to lower abundances. In the troposphere, thermal decomposition will reduce its concentration further and therefore HOONO is unlikely to influence tropospheric chemistry appreciably. Thus, unless other major sources of HOONO exist, it is unlikely to play a major role in the atmospheric photochemistry.

VI. CONCLUSIONS

We have observed both stable conformers of HOONO, *cis-cis* and *trans-perp*, formed as products in the reaction $OH+NO_2+M$ in a low pressure discharge flow cell. The two isomers are distinguished by their $2\nu_1$ overtone spectra recorded by action spectroscopy, leading to a new understanding of earlier tentative spectral assignments. The *trans-perp* HOONO $2\nu_1$ band is a sharp feature at 6971 cm^{-1}, observed only at temperatures below 240 K and at a frequency consistent with the spectrum reported by Pollack *et al.*[17] We have reassigned all of the bands observed in the room temperature overtone spectrum to *cis-cis* HOONO. We find that under thermal reaction conditions, the *trans-perp* isomer is initially formed at high, non-Boltzmann populations relative to *cis-cis* HOONO; the *trans-perp* HOONO then quickly isomerizes to the more stable *cis-cis* conformer.

We have studied the isomerization of *trans-perp* to *cis-cis* HOONO both experimentally and computationally. From our experimental measurements of the *trans-perp* HOONO decay, we find an isomerization lifetime of 39 ms at 233 K. From the isomerization data over the temperature range 223–238 K, we estimate the activation energy for *trans-perp* to *cis-cis* HOONO isomerization to be $E_{act}\sim33\pm12$ kJ/mol, consistent with a strong collision model as shown by statistical modeling. We have performed master equation modeling of the isomerization; we find a barrier height of 40.8 kJ/mol, consistent with experimental data. Finally, we have performed CCSD(T)/cc-pVQZ//CCSD(T)/cc-pVTZ *ab initio* calculations of the *perp-perp* HOONO isomer, the transition state for isomerization. We obtain an activation enthalpy of $\Delta H^{\ddagger0}_{298}=41.1$ kJ/mol, in good agreement with both experiment and statistical modeling.

We have calculated the $OH+NO_2$ photodissociation quantum yield as a function of excitation energy in the near-IR based on the best published *ab initio* and kinetics estimate of D_0(*cis-cis* HOONO)$=83$ kJ/mol, and find nonunity quantum yield predicted for some of the observed lower-frequency bands of *cis-cis* HOONO. We predict that the quantum yields should be sensitive to temperature, and that the apparent band strengths should change over the temperature range measured; however, we have not observed significant changes in the *cis-cis* HOONO spectrum from 193 to 273 K, suggesting that quantum yield is in fact unity for all bands. It is possible that relative intensity changes cannot be unambiguously observed with our present signal-to-noise ratios.

We have computed the relative transition strengths of the two conformers, and estimated the abundance of *trans-perp* HOONO relative to *cis-cis* HOONO. Semiempirical transition strength calculations using QCISD/AUG-cc-pVDZ level *ab initio* dipole moment functions predict that the $2\nu_1$ band of *trans-perp* HOONO absorbs more strongly than the $2\nu_1$ band of *cis-cis* HOONO, with a relative strength of 3.7 calculated using an anharmonic oscillator model and a relative strength of 3.2 calculated using a Morse oscillator model. B3LYP level calculations fail to produce reliable single-point calculations of dipole moment functions, while MP2, MP3, and QCISD level calculations predict consistent dipole moment functions. Using the calculated relative transition strength of *trans-perp* to *cis-cis* HOONO of 3.7:1 and assuming unit photodissociation quantum yield for both species, we determine an approximate upper bound on the initial *cis-cis* to *trans-perp* HOONO concentration ratio of 19:1.

The 213 K spectrum of *trans-perp* HOONO can be fit well to the predicted rotational constants, with a hybrid band ratio of 1.8:1 *a*-type to *c*-type, consistent with the simulation parameters that fit the Pollack *et al.*[17] jet-cooled spectrum. We support the assignment by Nizkorodov and Wennberg[11] of the 6365 cm^{-1} band to the origin of the *cis-cis* $2\nu_1$ overtone band. However, this band is broad and featureless, suggesting that *cis-cis* HOONO undergoes much more rapid IVR upon overtone excitation. We cannot make a definitive assignment of the remaining bands observed in the *cis-cis* spectrum.

Based on its calculated $2\nu_1$ transition strength, the more stable *cis-cis* HOONO is predicted to exist in the atmosphere at maximum concentrations of only 1.6×10^8 molecules cm^{-3} (80 pptv), and therefore, will be of limited importance in photochemical processes. For atmospheric chemistry, the most important impact of the formation of the short-lived HOONO reservoir is that the yield for radical loss via OH $+NO_2$ is not unity.

ACKNOWLEDGMENTS

This material is based upon work supported under a National Science Foundation Graduate Research Fellowship (J.L.F.) and supported by NSF's Atmospheric Chemistry program (Contract No. ATM-0094670) and the NASA Upper Atmospheric Research Program (Contract No. NAG5-11657). S.A.N. thanks the Camille and Henry Dreyfus Postdoctoral Program in Environmental Chemistry for support. The authors thank J. R. Barker for providing MULTIWELL input files and H. G. Kjaergaard, I. M. Konen, I. B. Pollack, E. X. J. Li, and M. I. Lester for insightful discussions.

[1] D. M. Golden and G. P. Smith, J. Phys. Chem. A **104**, 3991 (2000).
[2] D. M. Golden, J. R. Barker, and L. L. Lohr, J. Phys. Chem. A **107**, 11057 (2003).
[3] H. Hippler, S. Nasterlack, and F. Striebel, Phys. Chem. Chem. Phys. **4**, 2959 (2002).
[4] D. M. Matheu and W. H. Green, Int. J. Chem. Kinet. **32**, 245 (2000).
[5] J. Troe, Int. J. Chem. Kinet. **33**, 878 (2001).
[6] D. Fulle, H. F. Hamann, H. Hippler, and J. Troe, J. Chem. Phys. **108**, 5391 (1998).
[7] N. M. Donahue, R. Mohrschladt, T. J. Dransfield, J. G. Anderson, and M. K. Dubey, J. Phys. Chem. A **105**, 1515 (2001).
[8] J. S. Robertshaw and I. W. M. Smith, J. Phys. Chem. **86**, 785 (1982).
[9] B. D. Bean, A. K. Mollner, S. A. Nizkorodov, G. Nair, M. Okumura, S. P. Sander, K. A. Peterson, and J. S. Francisco, J. Phys. Chem. A **107**, 6974 (2003).
[10] D. A. Dixon, D. Feller, C. G. Zhan, and J. S. Francisco, J. Phys. Chem. A **106**, 3191 (2002).
[11] S. A. Nizkorodov and P. O. Wennberg, J. Phys. Chem. A **106**, 855 (2002).
[12] M. P. McGrath and F. S. Rowland, J. Phys. Chem. **98**, 1061 (1994).
[13] H. W. Jin, Z. Z. Wang, Q. S. Li, and X. R. Huang, Theochem-J. Mol. Struct. **624**, 115 (2003).
[14] H. H. Tsai, T. P. Hamilton, J. H. M. Tsai, M. vanderWoerd, J. G. Harrison, M. J. Jablonsky, J. S. Beckman, and W. H. Koppenol, J. Phys. Chem. **100**, 15087 (1996).
[15] Y. M. Li and J. S. Francisco, J. Chem. Phys. **113**, 7976 (2000).
[16] H. Hippler, S. Krasteva, S. Nasterlack, and F. Striebel (private communication).
[17] I. B. Pollack, I. M. Konen, E. X. J. Li, and M. I. Lester, J. Chem. Phys. **119**, 9981 (2003).
[18] R. S. Zhu and M. C. Lin, J. Chem. Phys. **119**, 10667 (2003).
[19] B. M. Cheng, J. W. Lee, and Y. P. Lee, J. Phys. Chem. **95**, 2814 (1991).
[20] P. O. Wennberg, R. C. Cohen, N. L. Hazen *et al.*, Rev. Sci. Instrum. **65**, 1858 (1994).
[21] S. Wu, G. A. Blake, Z. Y. Sun, and J. W. Ling, Appl. Opt. **36**, 5898 (1997).
[22] L. S. Rothman, C. P. Rinsland, A. Goldman *et al.*, J. Quant. Spectrosc. Radiat. Transf. **60**, 665 (1998).
[23] R. H. Judge and D. J. Clouthier, Comput. Phys. Commun. **135**, 293 (2001).
[24] R. A. Kenley, P. L. Trevor, and B. Y. Lan, J. Am. Chem. Soc. **103**, 2203 (1981).
[25] D. A. V. Kliner and R. L. Farrow, J. Chem. Phys. **110**, 412 (1999).
[26] M. J. Frisch, G. W. Trucks, H. B. Schlegel *et al.* GAUSSIAN 98, Revision A.9, 1998.
[27] K. Raghavachari, G. W. Trucks, J. A. Pople, and M. Head-Gordon, Chem. Phys. Lett. **157**, 479 (1989).
[28] T. H. Dunning, Jr., J. Chem. Phys. **90**, 1007 (1989).
[29] R. A. Kendall, T. H. Dunning, Jr., and R. J. Harrison, J. Chem. Phys. **96**, 6796 (1992).
[30] J. R. Barker, Int. J. Chem. Kinet. **33**, 232 (2001).
[31] N. M. Donahue, M. K. Dubey, R. Mohrschladt, K. L. Demerjian, and J. G. Anderson, J. Geophys. Res., [Atmos.] **102**, 6159 (1997).
[32] H. G. Kjaergaard, K. J. Bezar, and K. A. Brooking, Mol. Phys. **96**, 1125 (1999).
[33] H. G. Kjaergaard, C. D. Daub, and B. R. Henry, Mol. Phys. **90**, 201 (1997).
[34] H. G. Kjaergaard, B. R. Henry, and A. W. Tarr, J. Chem. Phys. **94**, 5844 (1991).
[35] H. G. Kjaergaard, H. T. Yu, B. J. Schattka, B. R. Henry, and A. W. Tarr, J. Chem. Phys. **93**, 6239 (1990).
[36] D. M. Turnbull, H. G. Kjaergaard, and B. R. Henry, Chem. Phys. **195**, 129 (1995).
[37] H. G. Kjaergaard, J. Phys. Chem. A **106**, 2979 (2002).
[38] J. W. Ochterski, Gaussian White Paper 1999.
[39] E. B. Wilson, J. C. Decius, and P. C. Cross, *Molecular Vibrations* (McGraw-Hill, New York, 1955).
[40] C. H. Choi and M. Kertesz, J. Phys. Chem. **100**, 16530 (1996).
[41] H. G. Kjaergaard, G. R. Low, T. W. Robinson, and D. L. Howard, J. Phys. Chem. A **106**, 8955 (2002).
[42] J. A. C. Gallas, Phys. Rev. A **21**, 1829 (1980).
[43] K. R. Lange, N. P. Wells, K. S. Plegge, and J. A. Phillips, J. Phys. Chem. A **105**, 3481 (2001).
[44] C. Chackerian, S. W. Sharpe, and T. A. Blake, J. Quant. Spectrosc. Radiat. Transf. **82**, 429 (2003).
[45] D. J. Donaldson, J. J. Orlando, S. Amann, G. S. Tyndall, R. J. Proos, B. R. Henry, and V. Vaida, J. Phys. Chem. A **102**, 5171 (1998).
[46] Z. M. Rong, H. G. Kjaergaard, and M. L. Sage, Mol. Phys. **101**, 2285 (2003).
[47] Z. Rong, D. L. Howard, and H. G. Kjaergaard, J. Phys. Chem. A **107**, 4607 (2003).
[48] R. J. Salawitch, P. O. Wennberg, G. C. Toon, B. Sen, and J. F. Blavier, Geophys. Res. Lett. **29**, 1762 (2002).
[49] C. W. Allen, *Allen's Astrophysical Quantities* (Springer, New York, 2000).
[50] T. F. Hanisco, E. J. Lanzendorf, P. O. Wennberg *et al.*, J. Phys. Chem. A **105**, 1543 (2001).